cmgh
CELLULAR AND MOLECULAR GASTROENTEROLOGY AND HEPATOLOGY

ORIGINAL RESEARCH

Differential MYC Phosphorylation Drives the Divergent Cholangiocyte Response to Stress

Steven P. O'Hara,* Patrick L. Splinter,* Antonia Felzen, Carys A. Turner, Olivia T. Morgenthaler, Gregory J. Gores, and Nicholas F. LaRusso

Division of Gastroenterology and Hepatology, Mayo Clinic, Rochester, Minnesota

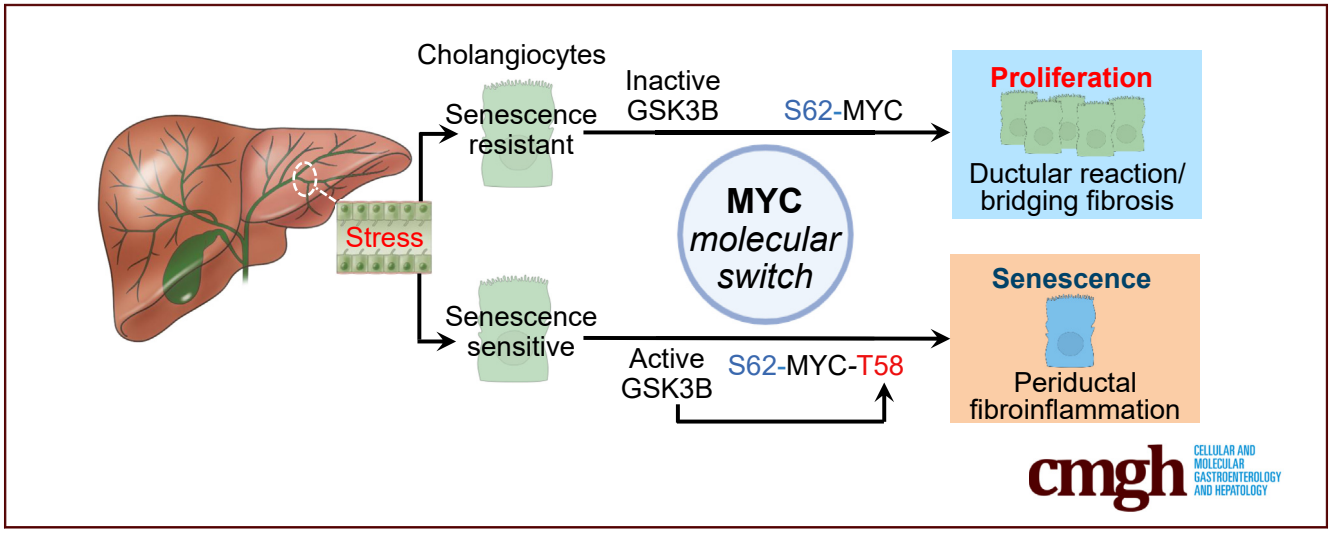

SUMMARY

Stress-induced MYC phosphorylation states promote either cholangiocyte proliferation (pS62) or senescence (pT58 via GSK3B). Our results identify MYC as a "molecular switch" in determining cholangiocyte responses to cellular stress and support that MYC activation drives cholangiocyte proliferation and ductular reaction.

BACKGROUND & AIMS: In primary sclerosing cholangitis (PSC), some cholangiocytes undergo cell cycle arrest (senescence), whereas others proliferate (ductular reaction). Our aim was to determine the mechanisms driving this divergent response.

METHODS: We analyzed PSC and control liver tissue by immunofluorescence for proliferative and senescent (sen) cholangiocytes. We used LPS to stress normal human cholangiocytes (NHCs) transfected with a senescence reporter ($p16_{prom}$-GFP) and fluorescence-activated cell sorting (FACS)-sorted sen (GFP+) or senescent-resistant (sen-res, GFP−) fractions. We performed RNA sequencing and quantitative polymerase chain reaction (qPCR) for senescence markers and immunoblots for phospho-(p)T58- MYC and pS62-MYC, and the kinase, GSK3B. Non-phosphorylatable MYC mutant NHCs were generated, and MYC or GSK3B were depleted or inhibited to assess effects on cell fate. MYC and GSK3B inhibitors were tested in 2 PSC mouse models (DDC and Mdr2-/-).

RESULTS: PSC tissue showed an overall increase in sen (∼2×), and proliferative (∼10×) cholangiocytes compared with controls, with senescence enriched in portal tracts and proliferation in parenchyma. RNA sequencing showed enrichment of MYC responsive genes in sen-res cholangiocytes ($P < .001$). Sen-res cholangiocytes showed increased total and pS62-MYC protein (∼3×), increased mRNA of the proliferation marker, *KI67* (>2.5×), and decreased *p16/p21* mRNA (∼75%). MYC inhibition in sen-res cholangiocytes promoted senescence (∼15×), whereas T58-MYC mutation reduced senescence and enhanced proliferation (∼3×). Sen cholangiocytes exhibited increased GSK3B (∼2×); GSK3B inhibition or depletion in sen-sensitive cholangiocytes reduced pT58-MYC and senescence (∼50%). In mouse models, MYC inhibition reduced, whereas GSK3B inhibition increased, cholangiocyte proliferation and fibrosis.

CONCLUSION: MYC phosphorylation promotes either cholangiocyte proliferation or senescence. The results reveal kinase mediators of cholangiocyte fate and identify MYC as a stress-responsive "molecular switch." *(Cell Mol Gastroenterol Hepatol 2025;19:101547; https://doi.org/10.1016/j.jcmgh.2025.101547)*

Keywords: Ductular Reaction; Primary Sclerosing Cholangitis; Proliferation; Senescence.

Primary sclerosing cholangitis (PSC) is a rare, incurable cholestatic liver disease characterized primarily by biliary inflammation and fibrosis. Disease progression

leads to biliary cirrhosis and liver failure.[1,2] The disease burden also includes a predisposition to hepatobiliary and colon cancer, is currently the 5th most common cause of liver transplantation, with a median survival time from diagnosis to death or transplant of 17 years.[3] Although our understanding of cell types, processes, and pathways involved in disease progression has improved, there remains no current effective therapeutic to slow or reverse disease progression. Further characterization of the cell types and molecular pathways driving PSC pathogenesis are requisite to identifying pharmaceutical targets for this syndrome.

The cholangiopathies, including PSC, are a group of diseases associated with cholestasis and bile duct destruction. The epithelial cells that line the bile ducts (cholangiocytes) are both a target and driver of PSC progression. We reported that cholangiocyte senescence (ie, permanent cell cycle arrest, apoptosis resistance, and a proinflammatory secretome) is a prominent feature of, and likely contributor to PSC pathogenesis and described epigenetic modifications influencing the senescent phenotype.[4–7] More recently, we proposed that the heterogeneity of cholangiocytes may influence distinct features of the disease, that is, both aberrant proliferation and senescence represent opposite pathologic fates of the reactive cholangiocyte in response to chronic injury.[8] The molecular mediators that determine whether a cholangiocyte, in response to cellular stressors, proliferates or becomes senescent remain ill-defined and is the focus of the work presented herein.

The functional heterogeneity of cholangiocytes has been recognized for decades. Broadly, cholangiocytes have been categorized as large or small, each possessing defined physiologic functions including proliferative capacity and bile acid modification capabilities.[9–11] More recently, single-nucleus RNA sequencing (snRNA-seq) has revealed multiple transcriptionally distinct cholangiocyte subpopulations,[12] yet the overlap and functional relevance of these populations remains to be fully explored. Our previous work demonstrating that cellular stressors induced senescence in some cholangiocytes, while inducing proliferation in others, each with a potential pathophysiologic role, led to the hypothesis that cholangiocyte cell fate uniquely influences disease progression. Here, we leveraged our in vitro model systems, in vivo models of PSC, and human liver tissue from PSC patients to identify the MYC proto-oncogene, BHLH transcription factor (MYC) as a driver of senescence resistance and the proliferative cholangiocyte phenotype and clarify the roles of the proliferative cell fate in PSC progression.

Results

Senescent and Proliferating Cholangiocytes Distribute Distinctly in Livers of Patients With PSC

We performed combined fluorescent *in situ* hybridization for cyclin-dependent kinase inhibitor 2A (*CDKN2A* [ie, *p16*, senescence marker]) and immunofluorescence for cytokeratin 7 (KRT7, cholangiocyte marker) and proliferating cell nuclear antigen (PCNA, proliferation marker). We assessed expression of *p16* and PCNA positivity, using average pixel intensity, from all KRT7 positive cholangiocytes in livers of patients without liver disease (non-disease) and patients with PSC. We found that both senescence and proliferation were increased in tissue samples from patients with PSC (Figure 1*A*). We next assessed expression of *p16* and PCNA positivity, by average pixel intensity within regions of interest (ie, KRT7-positive cholangiocytes from portal tracts [areas localized near portal vein and artery] vs KRT7 positive cholangiocytes within the parenchyma [ie, ductular reactive cholangiocytes]). We observed that senescent cholangiocytes accumulated in the portal tracts, whereas proliferative cholangiocytes were abundant in the parenchyma (Figure 1*B and C*). These data support that 2 cholangiocyte phenotypes exist in the livers of patients with PCS, those that senesce and those that proliferate.

Fluorescence-activated Cell Sorting Separates sen-sen From sen-res Cholangiocyte Populations

To further explore the phenotypic features of these distinct populations, we first transfected normal human cholangiocyte (NHC) with a *p16*-promoter driven green fluorescent protein (GFP) reporter (*p16*-GFP-NHC) and cultured these cells in the presence or absence of cellular stressors (lipopolysaccharide [LPS], hydrogen peroxide [H_2O_2], or irradiation (IR)] in our in vitro model of experimentally induced NHC senescence. Fluorescence-activated cell sorting (FACS) of unstimulated NHC revealed that ∼3% of the cholangiocytes exhibited GFP reporter positivity, whereas ∼30-40% of the cholangiocytes exposed to cellular stressors were positive for the *p16*-GFP reporter

***Authors share co-first authorship.**

Abbreviations used in this paper: **ANOVA, analysis of variance; ATACseq, assay for transposase-accessible chromatin using sequencing; C12FDG, 5-dodecanoylaminofluorescein di-β-D-galactopyranoside; ChIP, chromatin immunoprecipitation; DDC, 3,5-diethoxycarbonyl-1,4-dihydrocollidine; DMEM, Dulbecco's modified Eagle medium; DMYC,, depleted MYC; DR, ductular reaction; FACS, fluorescence-activated cell sorting; GFP, green fluorescent protein; GSEA, gene set enrichment analysis; GSK3b, glycogen synthase kinase 3b; H_2O_2, hydrogen peroxide; HBSS, Hank's Balanced Salt Solution; IFNA, interferon alpha; INFG, interferon gamma; IL, interleukin; IPA, Ingenuity Pathway Analysis; IR, irradiation; KRT7, cytokeratin 7; LPS, lipopolysaccharide; MSigDB, Molecular Signatures Database; NHC, normal human cholangiocyte; NOTCH1, Notch receptor 1; p16, cyclin-dependent kinase inhibitor 2A (CDKN2A); p21, CDKN1A; PBS, phosphate buffered saline; PCNA, proliferating cell nuclear antigen; PSC, primary sclerosing cholangitis; qPCR, quantitative polymerase chain reaction; RNA-seq, RNA sequencing; ROS, reactive oxygen species; S62, Serine 62; SA-bGAL, senescence-associated beta-galactosidase; SASP, senescence-associated secretory phenotype; SD, standard deviation; SDM, site-directed mutagenesis; sen, NHC experimentally induced to senescence; sen-res, NHC resistant to senescence; snRNA-seq, single-nucleus RNA sequencing; T58, Threonine 58; WT, wild-type; YAP, Yes-associated protein.**

Most current article

2352-345X
https://doi.org/10.1016/j.jcmgh.2025.101547

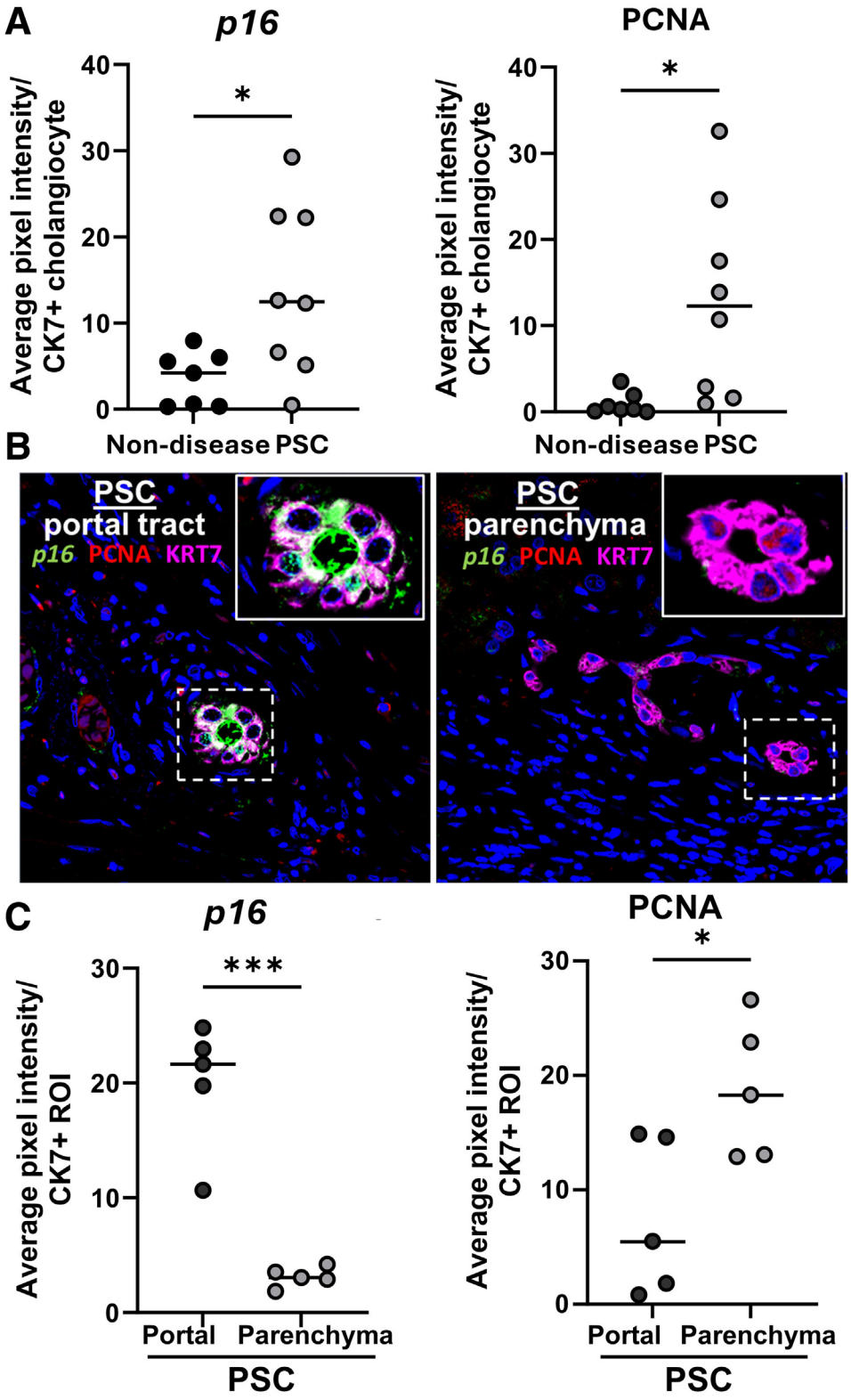

Figure 1. Senescent and proliferating cholangiocytes distribute distinctly in tissue from patients with PSC. (*A*) Quantitation of combined fluorescent in situ hybridization *CDKN2A* (ie, *p16*) and immunofluorescence for KRT7 and PCNA in PSC patient tissue. Both senescence (*p16*) and proliferation (PCNA) were increased in tissue samples from patients with PSC. (*B and C*) *p16* (*green*) and PCNA (*red*) positivity, by average pixel intensity, within regions of interest of tissue from patients with PSC (ie, portal tracts [areas localized near portal vein and artery]) vs KRT7 positive cholangiocytes within the parenchyma (ie, ductular reactive cholangiocytes). Senescent cholangiocytes accumulate in the portal tracts, whereas proliferative cholangiocytes were abundant in the parenchyma. $^{*}P < .05$; $^{***}P < .001$. n = 5 tissues from patients with late-stage PSC.

(LPS shown; Figure 2*A*). These results corresponded to the percent positive NHCs as assessed by the senescence-associated beta-galactosidase (SA-b-gal) assay (LPS shown; Figure 2*A*). Quantitative polymerase chain reaction (qPCR) confirmed an increase in senescence markers *p16* and cyclin dependent kinase inhibitor 1A (*CDKN1A* [ie, *p21*]) and a decrease in expression of the marker of proliferation *MKI67* (ie, *KI67)* in FACS GFP positive (GFP+) senescent (Sen)

compared to FACS GFP negative (GFP−) senescent resistant (sen-res) NHC treated with LPS (Figure 2*B*). Following a 24-hour incubation, we also collected media and performed a multiplexed antibody array to detect secreted proinflammatory/fibrogenic mediators. Densitometric analysis of analyte spots revealed that the GFP+ sen and GFP− sen-res

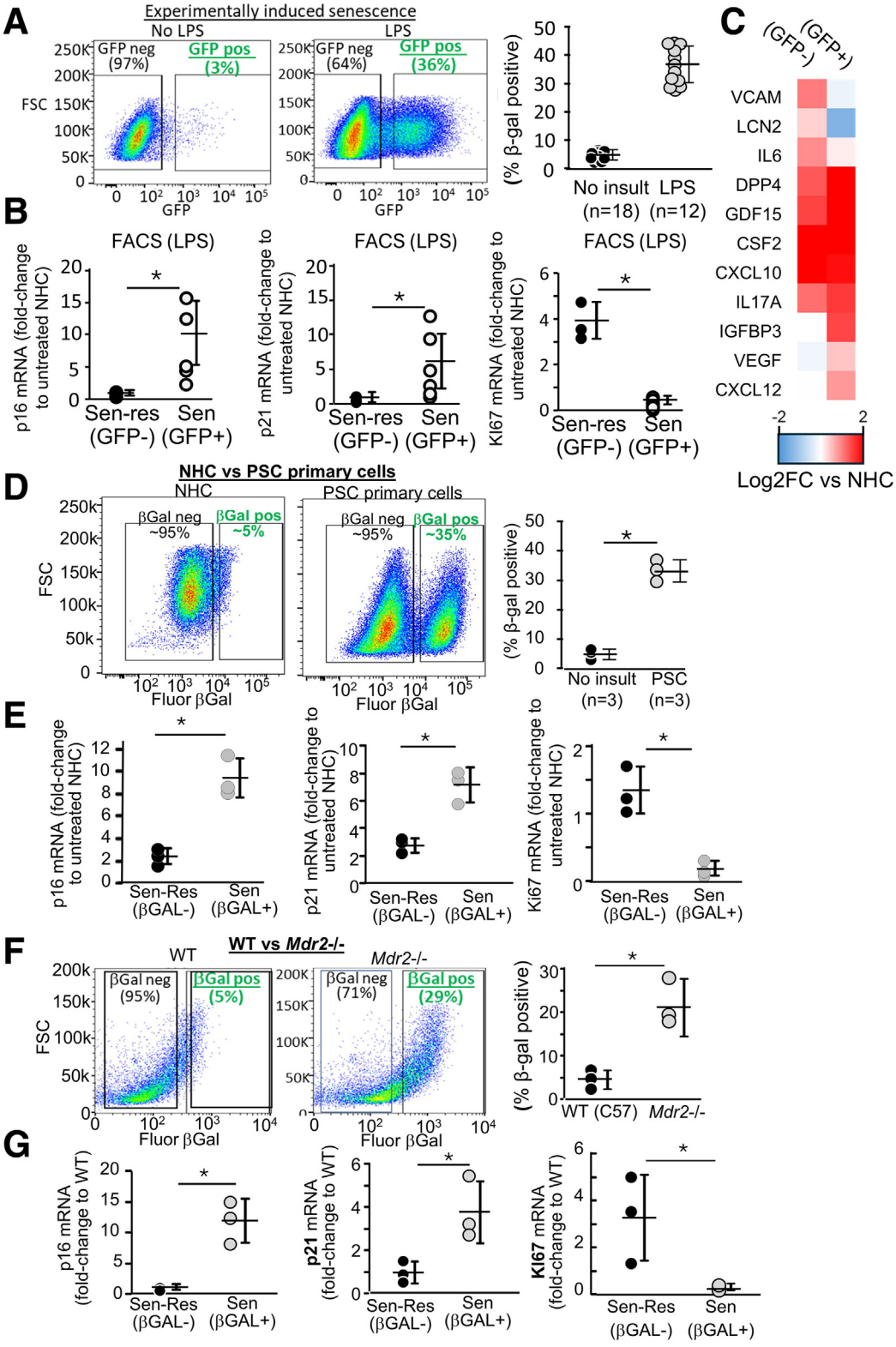

cholangiocytes exhibited overlapping, yet unique profiles (Figure 2*C*). We next FAC sorted, using fluorescent SA-b-gal, senescent from non-senescent cholangiocytes using control NHC and cholangiocytes isolated from explanted liver samples from patients with PSC. We again found that NHC exhibited ∼5% SA-b-gal-positive cholangiocytes, whereas cholangiocytes derived from patients with PSC exhibited ∼35% SA-b-gal-positive cholangiocytes (Figure 2*D*), consistent with what we have previously published in formalin-fixed paraffin-embedded tissues.[6] Again, the FAC-sorted SA-b-gal positive cholangiocytes derived from patients with PSC exhibited increased *p16* and *p21*, and decreased *KI67* compared with FAC-sorted SA-b-gal negative cholangiocytes derived from patients with PSC (Figure 2*E*). We next FAC-sorted senescent from non-senescent freshly isolated mouse cholangiocytes, using fluorescent SA-b-gal, from wild-type C57BL6 control (WT) and ATP Binding Cassette Subfamily B Member 4 (*Abcb4*) deficient mice (ie, *Mdr2*-/-), a well-accepted mouse model of sclerosing cholangitis. We found that ∼5% of the WT mouse cholangiocytes were fluorescent SA-b-gal-positive, whereas 20% to 25% of the *Mdr2*-/- mouse-derived cholangiocytes were SA-b-gal-positive. Moreover, SA-b-gal-positive FAC-sorted *Mdr2*-/- -derived cholangiocytes exhibited increased mRNA for *p16* and *p21*, and decreased *Ki67* expression compared with SA-b-gal-negative *Mdr2*-/- -derived cholangiocytes (Figure 2*F and G*).

We next FAC-sorted cholangiocytes stressed with either H_2O_2 or IR. Each stressor promoted a similar extent of SA-b-gal positivity, increased expression of senescence markers *p16* and *p21*, and decreased expression of the proliferation markers, *KI67* and *PCNA* (Figure 3*A and B*). Moreover, each stressor increased the expression of proinflammatory mediators, including interleukin (IL)8 and IL6, and the anti-apoptotic mediator, BCL2 Like 1 (*BCL2L1*, ie, BCL-xL) (Figure 3*C*). Western blot for the senescence marker, p21, confirmed increased senescence in LPS-treated, FAC-sorted GFP+ NHC vs GFP− NHC (Figure 3*D*). We next cultured NHC and FAC-sorted GFP+ sen and GFP− sen-res cholangiocytes. We found that GFP+ cholangiocytes exhibited increased size, mitochondrial mass, reactive oxygen species concentration, and decreased mitochondrial membrane potential compared with FAC-sorted GFP− sen-res cholangiocytes (Figure 3*E*). Additionally, we found that the FAC-sorted GFP− sen-res population resisted senescence induction following extended exposure to LPS or H_2O_2 (24 days; Figure 3*F*). These results support that we can separate 2 distinct populations of NHCs that either continue to proliferate or transition to senescence upon exposure to cellular stress.

Clonally Isolated NHCs Are Either Sensitive or Resistant to Stress-induced Senescence

Having demonstrated that stressed NHC, PSC patient-derived, and *Mdr2*-/- mouse cholangiocytes can be separated into both non-senescent/proliferative and senescent cholangiocytes, we next asked whether clonally isolated NHC were either susceptible or resistant to cellular stress-induced senescence. To achieve this, we isolated and expanded a total of 118 *p16*-GFP-NHC cholangiocyte clones prior to cellular stress (Figure 4*A*). Using our in vitro model of induced senescence, we next assessed whether these clonally derived NHC were resistant (sen-res) or sensitive (sen-sen) to cellular-stress induced senescence. Using fluorescent microscopy to detect the GFP reporter, we found that individual clones were either resistant (eg, clone 28) or susceptible (∼90% senescent [eg, clone 80]) to H_2O_2 or LPS-mediated cellular stress. Western blotting for the senescence marker, p21, confirmed resistance (clone 28) or susceptibility (clone 80) to LPS-induced senescence (Figure 4*B*). Using qPCR of clonal isolates cultured in our in vitro model of experimentally induced senescence, we further showed that sen-sen clone 80, but not sen-res clone 28 exhibited increased *p16* and *p21* mRNA, when cultured in the presence of LPS, conversely, sen-res clone 28 exhibited increased expression of the proliferation marker, *KI67*, whereas sen-sen clone 80 exhibited decrease *KI67* expression in the presence of LPS (Figure 4*C*). Next, we transfected sen-res and sen-sen clones with a luciferase reporter, exposed the transfected cells to LPS for 10 days, injected them into explanted mouse liver lobes maintained in growth media, and tracked growth of the cholangiocytes by luciferin treatment and

Figure 2. (***See previous page***). **FAC sorting separates sen-sen from sen-res cholangiocytes.** (*A*) FACS of NHC transfected with a *p16*-promoter driven GFP reporter. Approximately 40% of the cholangiocytes exposed to cellular stressors (LPS shown) were positive for the p16-GFP reporter. SA-b-gal assay supported increased senescence in LPS treated cholangiocytes. (*B*) qPCR of sorted sen and sen-res population. The senescent markers *p16* and *p21* were increased, whereas the proliferation marker *KI67* was decreased in senescent (Sen) compared with FAC-sorted GFP negative (GFP−) senescent resistant (sen-res) NHCs treated with cellular stressors LPS. (*C*) Multiplex antibody array to detect secreted proinflammatory/fibrogenic mediators in conditioned media. Densitometric analysis of analyte spots revealed overlapping, yet unique profiles in sen vs sen-res populations. (*D*) Fluorescent SA-β-gal detection of senescence in NHCs vs PSC primary cells. NHCs exhibited ∼5% SA-b-gal-positive cholangiocytes, whereas PSC patient-derived cholangiocytes exhibited ∼35% SA-b-gal-positive cholangiocytes. SA-b-gal colorimetric assay of cells in culture confirmed an increase in senescence. (*E*) qPCR of sorted sen and sen-res PSC patient cholangiocytes. The senescent markers *p16* and *p21* were increased, whereas the proliferation marker KI67 decreased in SA-b-gal-positive PSC patient-derived cholangiocytes compared with FAC-sorted PSC patient-derived SA-b-gal-negative cholangiocytes. (*F*) Fluorescent SA-β-gal detection of senescence in freshly isolated WT and *Mdr2*-/- mouse cholangiocytes. WT mice exhibited ∼ 5% SA-β-gal-positive cholangiocytes, whereas *Mdr2*-/- mice exhibited ∼ 30% SA-β-gal-positive cholangiocytes. (*G*) qPCR of sorted sen-res and sen *Mdr2*-/- cholangiocytes. The senescent markers *p16* and *p21* were increased, whereas the proliferation marker *Ki67* decreased in SA-β-gal-positive *Mdr2*-/- mouse cholangiocytes compared with FAC-sorted *Mdr2*-/- mouse-derived SA-β-gal-negative cholangiocytes.

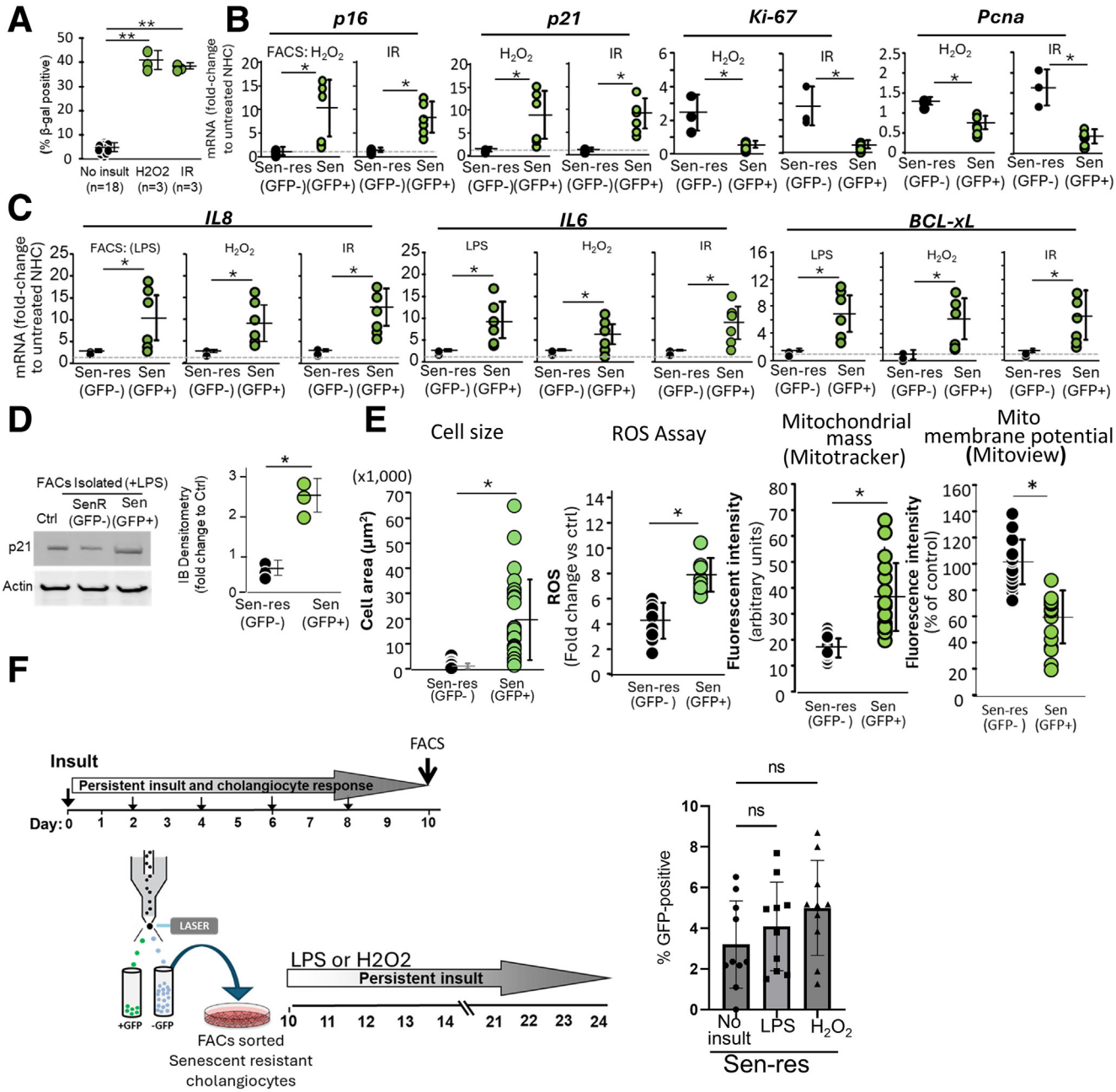

Figure 3. Characteristics of FAC-sorted senescent cells. (*A*) H_2O_2 and IR induced senescence in ~40% of the NHCs. (*B*) qPCR demonstrated increased senescence and decreased proliferation markers in IR and H_20_2-induced NHC senescence. (*C*) qPCR for *IL8*, *IL6*, and the anti-apoptosis mediator, *Bcl-xL*, demonstrating increased expression in LPS-, IR-, and H_2O_2-induced NHC senescence. (*D*) Western blot demonstrates increased p21 expression in LPS induced senescent NHCs. (*E*) Phenotypic characteristics of LPS-induced senescent cholangiocytes. (*F*) The FAC-sorted senescent resistant NHCs continued to grow in the extended presence (24 days) of LPS or H_2O_2.

luminescence measurements using an in vivo imaging system. We found, as expected, that the sen-sen clone showed no luminescence, whereas the sen-res clone exhibited increased luminescence, indicating continued growth (Figure 5). These results from clonally isolated NHCs support the presence of distinct populations of cholangiocytes that are either resistant or susceptible to cellular-stress induced senescence.

Sen-res Cholangiocytes are Characterized by a MYC-driven Gene Expression Profile

To begin to address pathways that may promote resistance or sensitivity to stress-induced senescence, we performed bulk RNA sequencing (RNAseq) on unstimulated *p16*-GFP-NHC, and *p16*-GFP-NHC treated with LPS and FAC sorted into sen-res (GFP−) and sen (GFP+) populations. Differential gene expression, visualized by volcano plots,

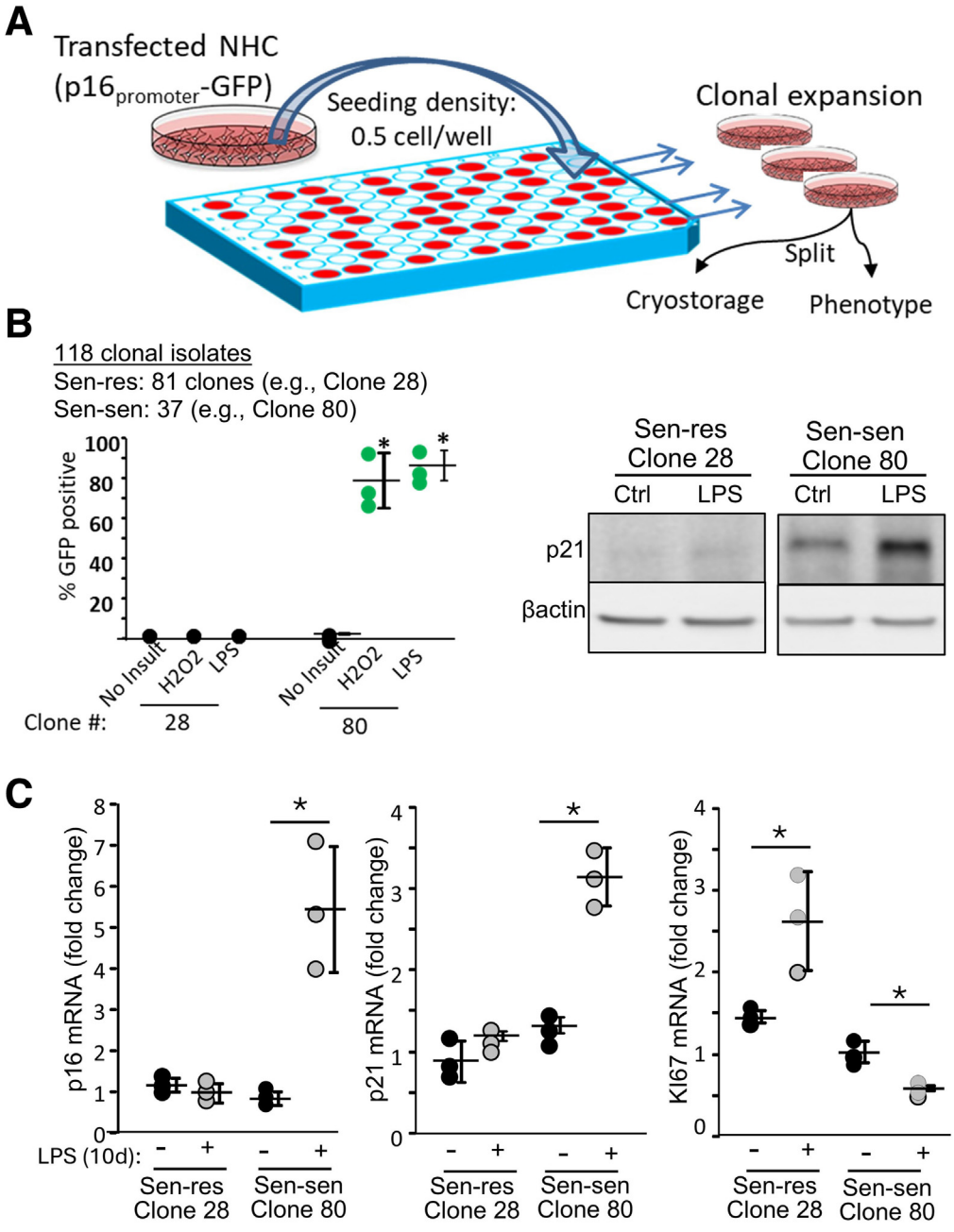

Figure 4. Clonal isolation of NHCs results in senescence-sensitive and -resistant cholangiocyte populations. (*A*) Schema of clonal isolation of cholangiocytes transfected with the senescence reporter p16 promoter - GFP. (*B*) Clones were either resistant (eg, clone 28) or sensitive (eg, clone 80) to H_2O_2- and LPS-driven senescence as demonstrated by p16-GFP positivity. Western blotting for p21 confirmed resistance (clone 28) or susceptibility (clone 80) to LPS-induced senescence. (*C*) qPCR of senescence and proliferation markers. Sen-sen clone 80, but not sen-res clone 28 exhibited increased *p16* and *p21* mRNA, and decreased *KI67* when cultured in the presence of LPS.

demonstrates that sen cholangiocytes exhibited 745 genes that were significantly reduced (Log2FC ≤ -1; $-$Log10FDR >1.3) and 1877 genes that were significantly increased compared with sen-res cholangiocytes (Figure 6*A*). We next performed gene set enrichment analysis (GSEA)[13,14] using the Molecular Signatures Database (MSigDB) Hallmark Gene Set Collection[15] to assess whether any defined gene sets (ie, groups of genes with defined biological function) are enriched in either of the 2 populations. We found 2 Hallmark Gene Sets that are upregulated in the sen-res compared with the sen population (nominal *P*-value $< .01$; FDR $< .25$) including MYC Targets V1 (194 genes in the gene set, 136 enriched [136/194]) and MYC Targets V2 (42/58 enriched) (Figure 6*B*). Conversely, we found 16 Hallmark Gene Sets that are upregulated in sen compared with the sen-res population, the top 3 gene sets being interferon alpha (*INFA*) response (71/95 enriched) (Supplementary Table 1), interferon gamma (*INFG*) response (129/198 enriched), and p53 pathway (116/193 enriched). Given that we obtained limited numbers of primary PSC patient cholangiocytes for further analysis, we performed GSEA of previous bulk RNA-seq data comparing NHCs with PSC patient-derived cholangiocytes.[7] We found that 9 Hallmark Gene Sets were enriched in unstimulated NHCs compared with PSC patient-derived

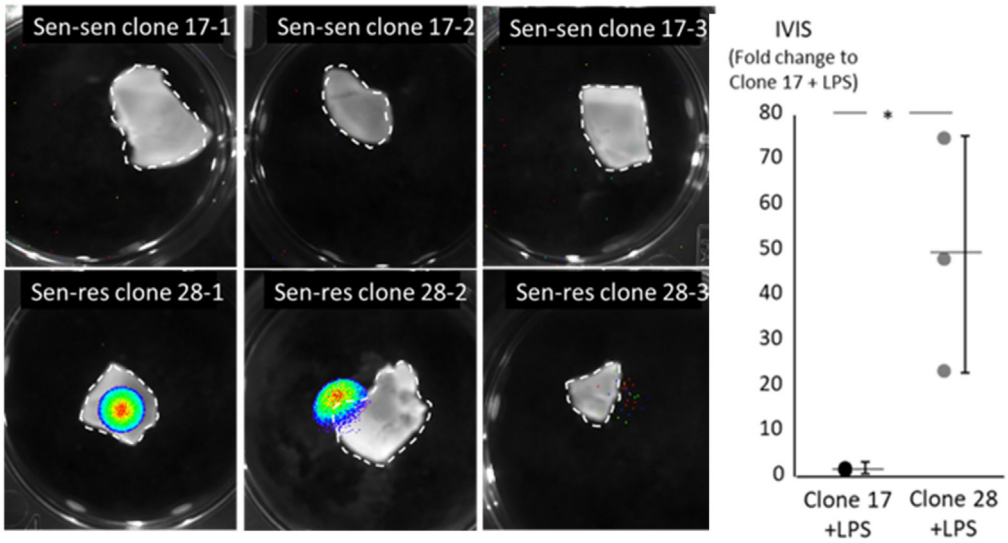

Figure 5. Luminescence of implanted sen and sen-res cholangiocytes. Clonally derived sen-sensitive and sen-resistant cholangiocytes were stably transfected with a luciferase reporter and exposed to LPS for 10 days. The treated cells were injected into explanted mouse liver lobes maintained in growth media for 5 days and exposed to luciferin. The sen-sen clone showed no luminescence, whereas the sen-res clone exhibited increased luminescence, indicating continued growth. Luminescence readings were performed using IVIS Spectrum imaging.

cholangiocytes, including MYC Targets V1 and 2. Additionally, 19 Hallmark Gene Sets were enriched in PSC patient-derived cholangiocytes, including *INFA* (43/95 enriched) (Supplementary Table 1) *INFG* response (75/198 enriched), and p53 pathway (71/193 enriched).

To further define potential pathways differentiating sen and sen-res populations, we performed Ingenuity Pathway Analysis (IPA) and assessed upstream activators that define sen and sen-res (representative upstream regulators shown in Figure 6*C*). We found 15 upstream regulators with a significant Z-score (absolute Z-score >2, denoted by asterisks) in sen vs sen-res. Inhibition of the upstream activator, MYC, was the strongest signal defining downregulated genes in the sen vs the sen-res cholangiocytes (ie, upregulated in sen-res, Z score <−6.0, *P*-value of overlap < 8.0E-23) (Figure 6*C*; Supplementary Table 2). Conversely, activation of the upstream factors, *INFG* and *IFNA*, were the strongest signal defining upregulated genes in sen vs the sen-res cholangiocytes (Z scores >8.0 and *P*-value of overlap < 5.0E-54). Moreover, we demonstrate that depletion of MYC (CRISPR/cas9) in NHC diminishes LPS-induced MYC target gene expression (Figure 7). Together these data support that at least 2 populations of cholangiocytes exist (ie, those that are sensitive to and those that are resistant to senescence); and that these populations are characterized by either loss of MYC activation in sen cholangiocytes or increased MYC activation in the sen-res population.

The MYC Inhibitor, MYCi975, diminishes cholangiocyte Proliferation in Mouse Models of PSC

Having demonstrated that MYC-driven gene expression is a feature of sen-res NHCs, we hypothesized that MYC inhibition would diminish cholangiocyte proliferation (ductular reactive cells) and reduce bridging fibrosis in mouse models of PSC. We first assessed, by immunofluorescence, portal vs parenchymal cholangiocyte MYC expression in 3,5-diethoxycarbonyl-1,4-dihydrocollidine (DDC)-fed and *Mdr2-/-* mice. We found that MYC expression is increased ~2- to 3-fold in the parenchymal cholangiocytes compared with cholangiocytes localized to the portal tracts in both mouse models (Figure 8*A*). Picrosirius red staining revealed that DDC-fed and *Mdr2-/-* mice treated with vehicle exhibited increased fibrosis compared with mice fed normal chow, whereas treatment with MYCi975 clearly showed reduced fibrosis in DDC-fed mice and suggested diminished bridging fibrosis in the *Mdr2-/-* mice (Figure 8*B*). Quantitation revealed a >70% reduction in Sirius red staining in MYC inhibitor-treated DDC-fed mice compared with DDC-fed vehicle-treated mice; whereas Sirius red staining in MYC inhibitor treated *Mdr2-/-* mice trended towards ($P = .133$) but did not reach significance (Figure 8*C*). Finally, we assessed ductular reaction, by quantitating total KRT7 positivity, percent PCNA-positive (proliferation marker) cholangiocytes, and mRNA expression of *Krt7*, *Pcna* (proliferation), and *p16* (senescence) in the livers. We found that total KRT7 positivity and the percentage of PCNA-positive cholangiocytes was increased in DDC-fed mice compared with mice fed normal chow, whereas DDC-fed and *Mdr2-/-* mice treated with MYCi975 exhibited reduced KRT7 expression and reduced PCNA-positive cholangiocytes throughout the tissue (Figure 8*D*). Moreover, MYCi treatment reduced *Krt7* and *Pcna* mRNA and increased *p16* mRNA expression (Figure 8*E*). *Mdr2-/-* mice also showed reduced KRT7 positivity, PCNA-positive cholangiocytes, and a similar reduction of *Krt7* and *Pcna* mRNA and increased *p16* mRNA expression following MYCi treatment (Figure 8*F and G*). Serum biochemistries

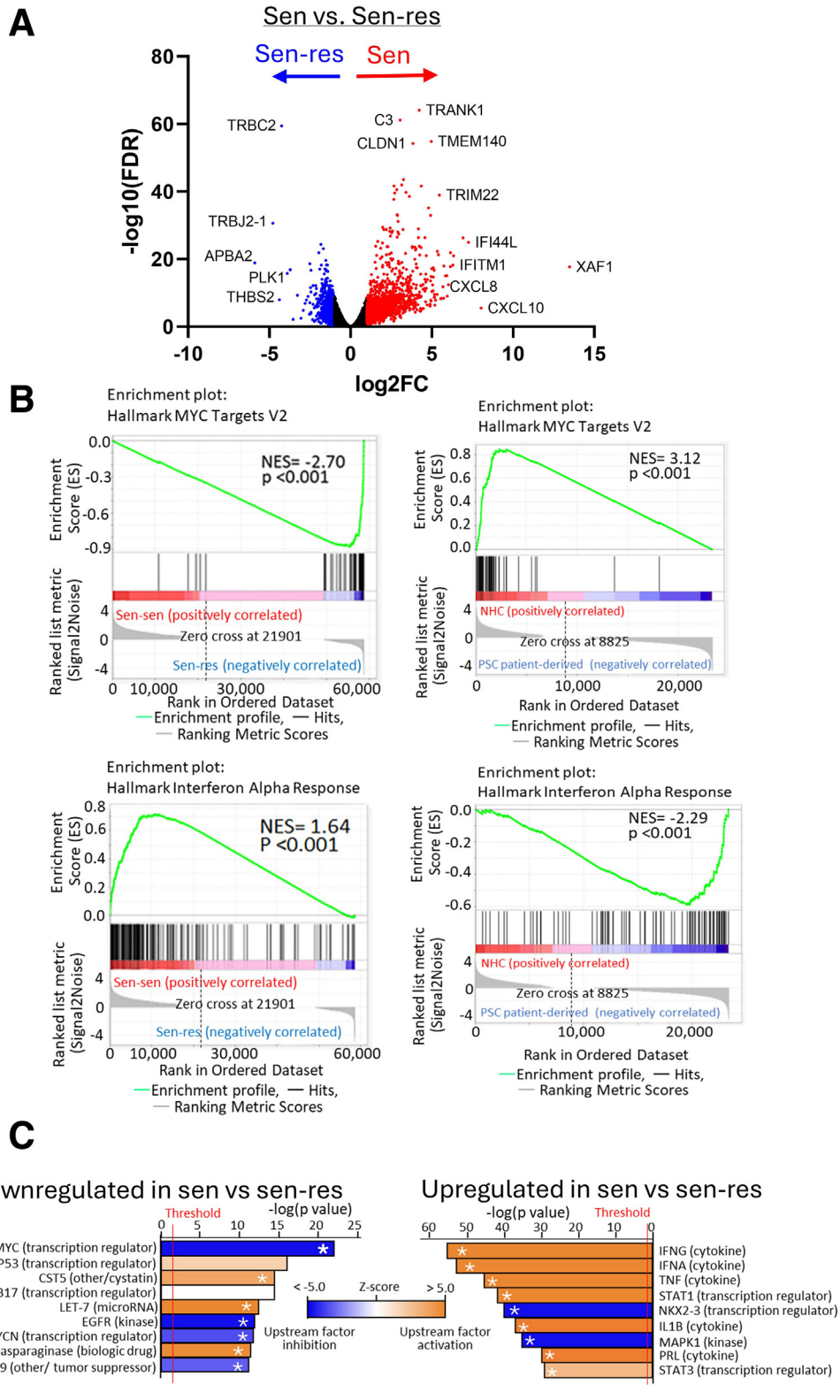

Figure 6. Bulk RNA-seq demonstrates that the sen-res cholangiocytes are characterized by a MYC-driven gene expression profile. (*A*) Volcano plots showing that sen-sen cholangiocytes exhibited 745 genes that were significantly reduced (Log2FC ≤ -1; $-$Log10FDR >1.3) and 1877 genes that were significantly increased compared with sen-res cholangiocytes. (*B*) GSEA revealed that MYC targets are upregulated, whereas IFNA response genes are downregulated in the sen-res compared with the sen population (nominal *P*-value $<$ .01, FDR <0.25) and in NHCs vs primary PSC patient cholangiocytes. (*C*) IPA revealed the upstream activators that define sen and sen-res. Inhibition of the upstream activator, MYC, was the strongest signal defining downregulated genes in the sen vs the sen-res cholangiocytes (ie, upregulated in sen-res, Z score <-6.0, *P*-value of overlap $<$ 8.0E-23). Conversely, activation of the upstream factors, INFG and IFNA, were the strongest signal defining upregulated genes in sen vs the sen-res cholangiocytes (Z scores >8.0 and *P*-value of overlap $<$ 5.0E-54).

revealed improved total alkaline phosphatase, alanine aminotransferase, total bilirubin, and total bile acids in the DDC-fed MYC inhibitor-treated mice compared with vehicle-treated mice (Figure 9). Together, these data support that MYC is a central driver of cholangiocyte ductular reaction and may contribute to fibrosis.

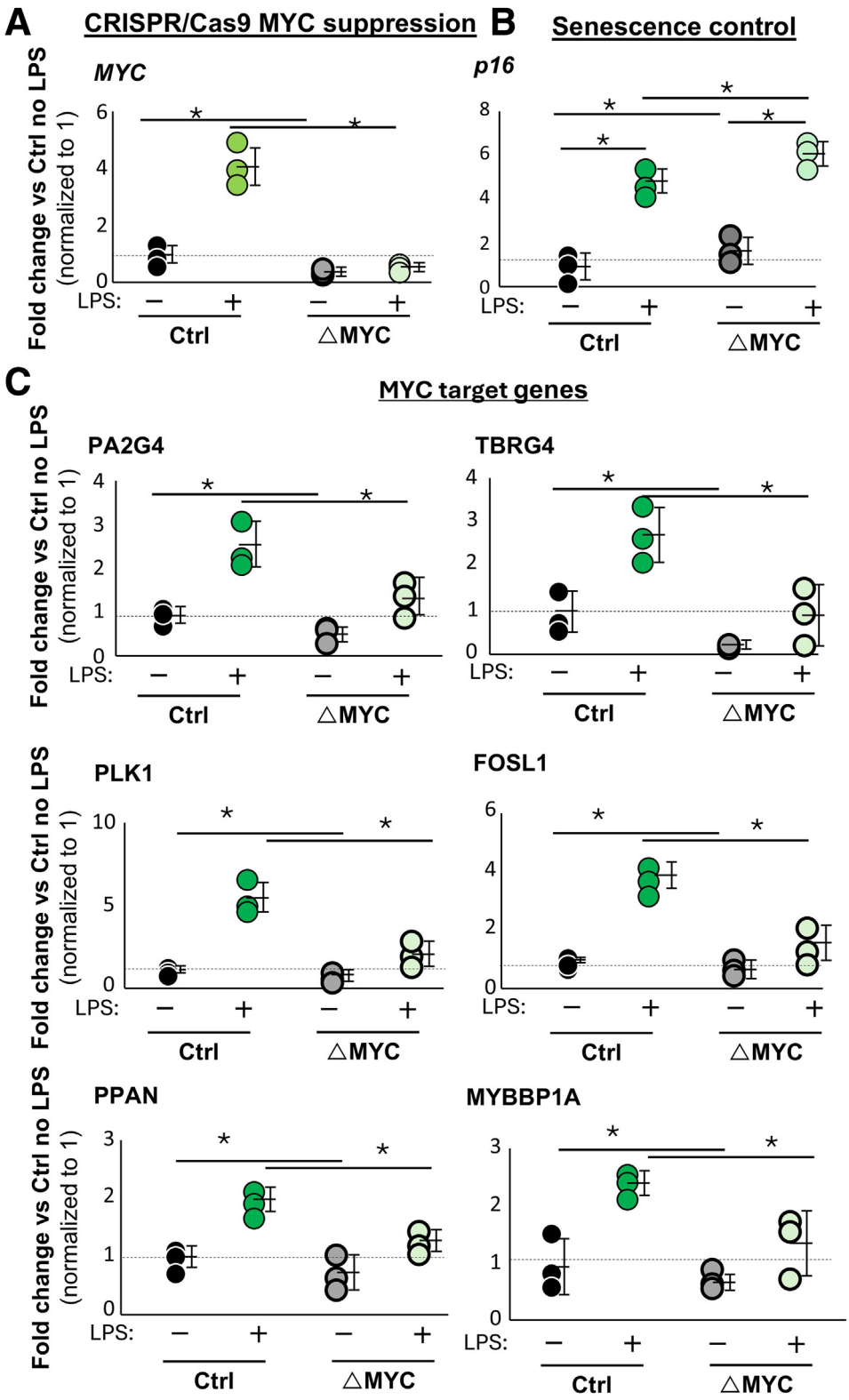

Figure 7. CRISPR/Cas9 deletion of *MYC* in NHC. (*A*) qPCR demonstrates that *MYC* is depleted. *MYC* mRNA is increased in induced senescent control NHCs but not in *MYC* depleted cells (DMYCs). (*B*) qPCR demonstrates that *MYC* depletion promotes senescence in NHCs. (*C*) qPCR showing that depletion of *MYC* suppresses MYC target gene expression. *$P < .05$.

Sen and sen-res Cholangiocytes Exhibit Differential MYC Phosphorylation

MYC is post-translationally modified by phosphorylation at 2 critical sites; Serine 62 (S62) phosphorylation stabilizes the MYC protein, whereas Threonine 58 (T58) phosphorylation marks the protein for proteasomal degradation.[16,17] Having shown the functional relevance of MYC in proliferating cholangiocytes and the ductular reaction,

we next assessed whether MYC protein is increased in FACS isolated sen-res vs sen cholangiocytes and whether the MYC protein is differentially phosphorylated between the 2 subpopulations following LPS-mediated stress. Our RNA-seq data supports that MYC gene expression is elevated in sen-res vs sen cholangiocytes; we confirmed this observation by

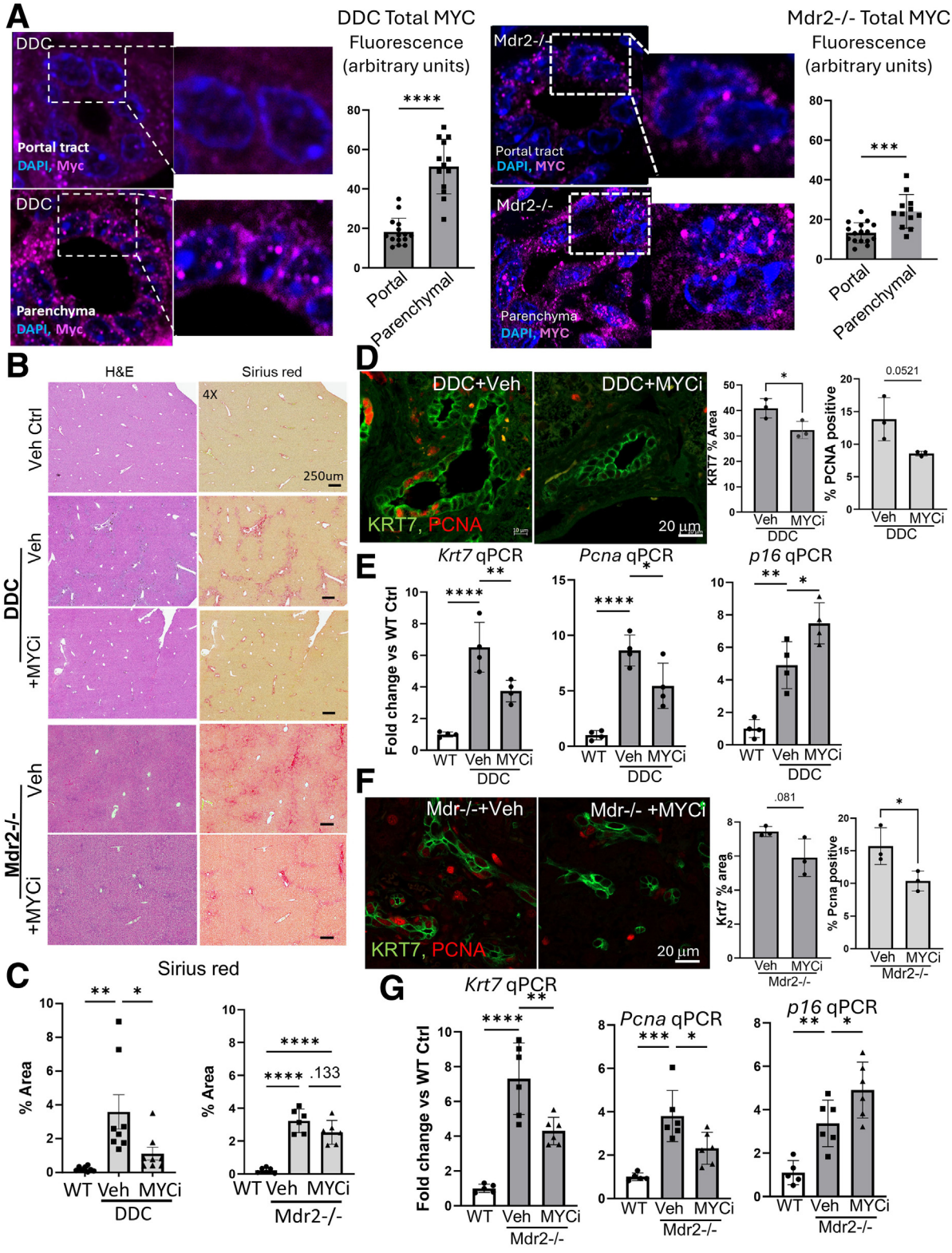

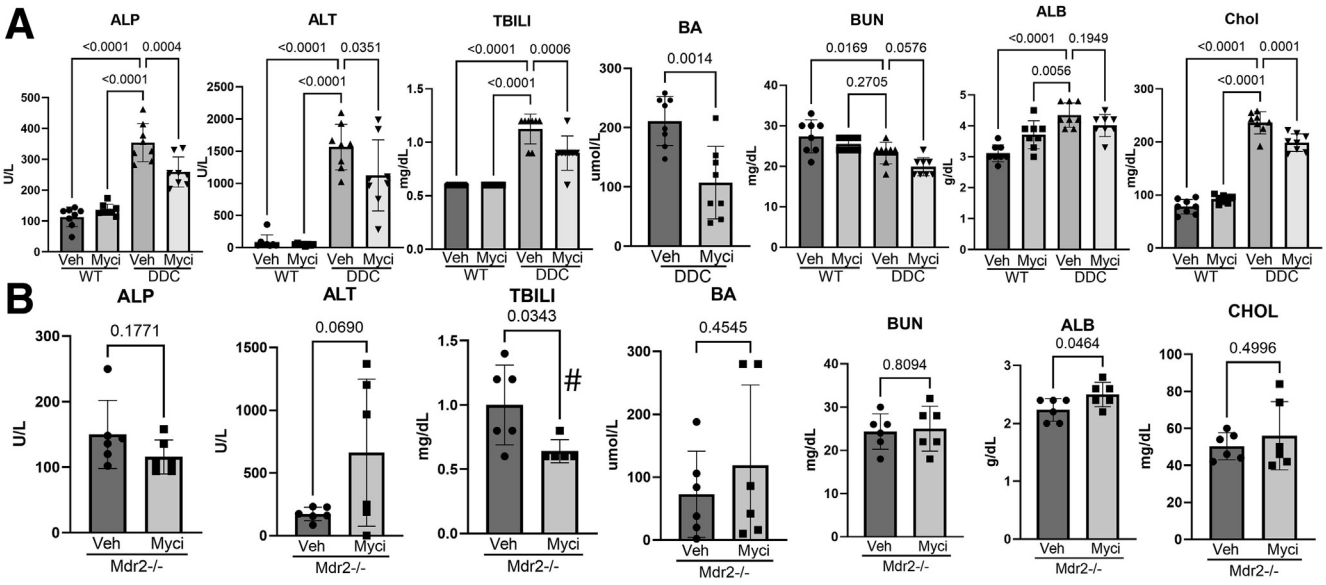

#, outlier removed ([ROUT (Q=0.5%)], TBILI, Mdr2-/- Myci, 2.6 mg/dL

Figure 9. Serum biochemistries in the presence and absence of MYC inhibitor, MYCi975. (*A*) DDC-fed mice exhibited increased serum alkaline phosphatase (ALP), alanine aminotransferase (ALT), total bilirubin (TBILI), total bile acids (BA). albumin (ALB), and cholesterol (CHOL). DDC-fed mice treated with the MYCi975 (Myci) exhibited a decrease in ALP, ALT, TBILI, BA, and CHOL. (*B*) *Mdr2-/-* mice treated with MYCi exhibited a trend towards decreased ALP, and significantly reduced TBILI.

qPCR (Figure 10*A*). We further show, by immunoblot, that total MYC protein is increased in sen-res vs sen cholangiocytes (Figure 10*B*). Moreover, we demonstrate, by immunoblot, that S62 phosphorylation is increased in FACS-isolated sen-res vs sen cholangiocytes, and, conversely, that T58 phosphorylation is increased in the sen vs sen-res population (Figure 10*B and C*). We next asked, using our model of induced cholangiocyte senescence, whether clonal isolates of sen-res and sen cholangiocytes exhibited different phosphorylation patterns. Again, using immunoblotting, we found that the sen-res clone (clone 28), but not the sen-sen clone (clone 80), exhibited increased S62 phosphorylation (~1.5-fold increase), whereas clone 80, but not clone 28, exhibited increased T58 phosphorylation (~2-fold increase) following LPS-mediated stress (Figure 10*D*). Quantitation of the immunoblots, normalized to total actin, is shown in Figure 10*E*. These results support that MYC expression (both RNA and protein) is increased in sen-res cholangiocytes and that MYC phosphorylation patterns differ between sen-res and sen cholangiocytes.

To validate the relevance of S62 and T58 phosphorylated residues in driving cholangiocyte cell fate (ie, proliferation or senescence), we depleted MYC in NHCs using CRISPR/Cas9 (DMYC) and reconstituted the cells with MYC constructs that either promoted overexpression of WT MYC, or non-phosphorylatable MYC mutants (S62 to Alanine [S62A] and T58 to Alanine [T58A]). By immunoblot, we found that DMYC cholangiocytes (~70% reduction of MYC), cultured in the absence of LPS insult, exhibited increased p21 expression (~3-fold) compared with WT NHCs cultured in the absence of LPS; additionally,

Figure 8. (*See previous page*). The MYC inhibitor, MYCi975, diminishes cholangiocyte proliferation in mouse models of PSC. (*A*) Immunofluorescence for portal vs parenchymal cholangiocyte MYC expression in livers from DDC-fed and *Mdr2-/-* mice. MYC expression is increased ~2-fold in the parenchymal cholangiocytes compared with cholangiocytes localized to the portal tracts in both animal models. (*B*) Representative images of H&E-stained liver sections showing parenchyma and portal tracts of vehicle-treated WT control (Veh Ctrl; n = 8), DDC-fed plus vehicle (Veh; n = 8), DDC-fed Myc inhibitor-treated (MYCi; n = 8), *Mdr2-/-* (n = 6), and *Mdr2-/-* MYC inhibitor-treated (n = 6) mice (*left panels*) and Picrosirius-red-stained liver sections (magnification: 4×) showing deposition of collagen (*right panels*). (*C*) Quantitation of Picrosirius reveals a significant reduction in fibrosis in MYC inhibitor-treated DDC-fed mice, and a trend towards significance ($P = .133$) in MYC inhibitor-treated *Mdr2-/-* mice. Data is presented as the percentage of Picrosirius-positive/total image area. (*D*) Immunofluorescence of KRT7 and PCNA in DDC-fed mice. KRT7 (KRT7-positive/total image area) and percentage of cholangiocytes positive for PCNA were reduced in mice treated with the MYC inhibitor. (*E*) qPCR for total liver *Krt7*, *Pcna*, and *p16* in WT C57BL6, DDC-fed, and DDC-fed MYCi-treated mice. Total liver *Krt7* and *Pcna* mRNA are reduced, whereas total liver *p16* is increased in MYCi treated DDC-fed mice vs DDC-fed vehicle mice. (*F*) Immunofluorescence of KRT7 and PCNA in *Mdr2-/-* mice. Total KRT7 trended towards significance, and percentage of cholangiocytes positive for PCNA was reduced in *Mdr2-/-* mice treated with the MYC inhibitor. (*G*) qPCR for total liver *Krt7*, *Pcna*, and *p16* in WT C57BL6, *Mdr2-/-*, and *Mdr2-/-* MYCi treated mice. Total liver *Krt7* and *Pcna* mRNA are reduced, whereas total liver *p16* is increased in MYCi treated *Mdr2-/-* vs vehicle-treated *Mdr2-/-* mice. *$P < .05$; **$P < .01$; ***$P < .001$; ****$P < .0001$.

proliferation, as measured by MTS assay, was reduced by 50% (Figure 10*F and G*). Using our model of LPS-induced senescence (ie, +LPS), we found, by immunoblot, that DMYC cholangiocytes exhibited increased p21 expression (~4-fold) compared with NHCs and exhibited increased percentage (1.5-fold) of cholangiocytes positive for the senescence marker SA-b-gal (Figure 10*F and G*). In the absence of LPS, reconstitution of the DMYC cholangiocytes

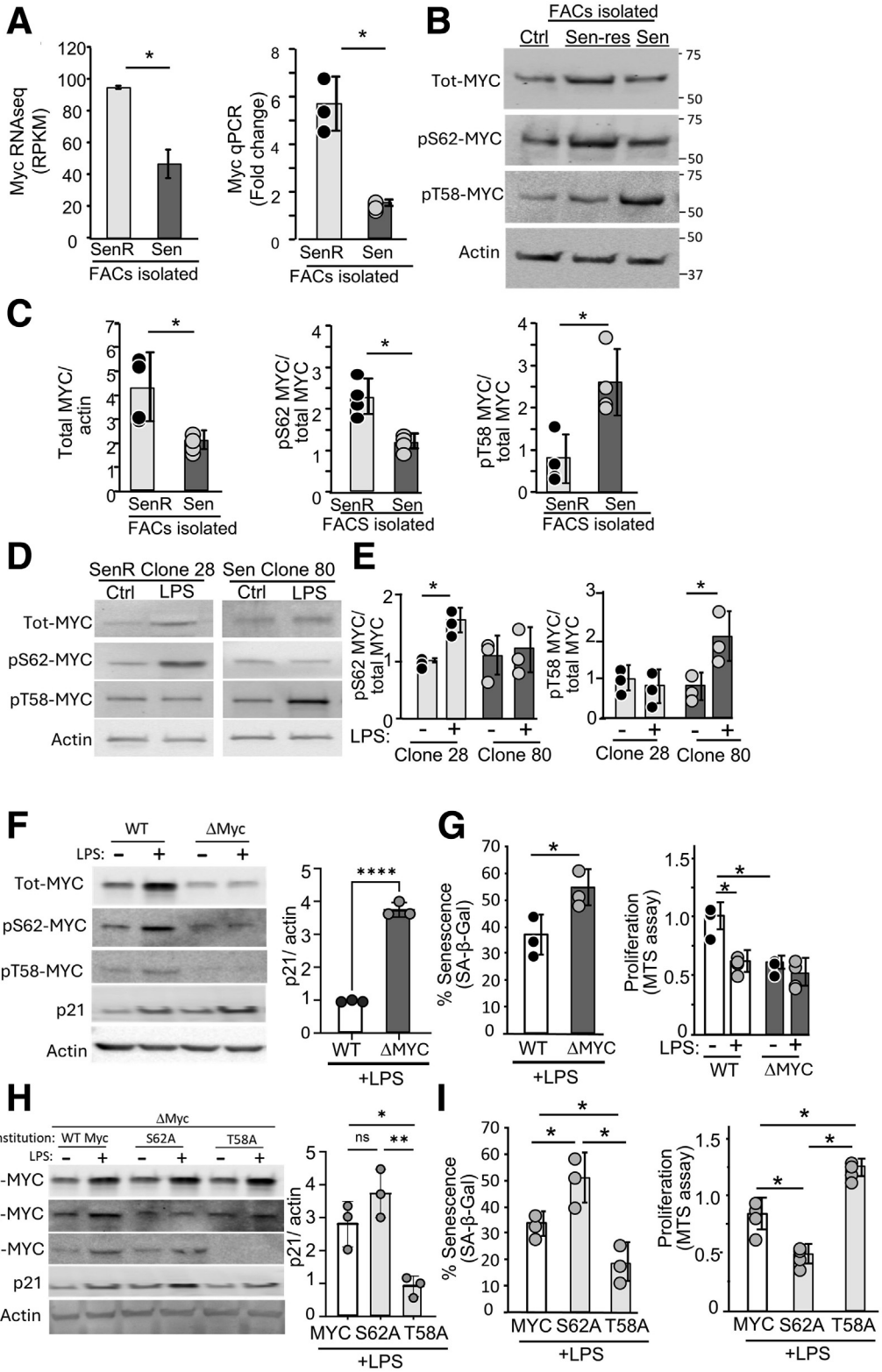

with plasmids encoding the non-phosphorylatable mutant MYC S62A exhibited increased p21 expression (Figure 10*H*). Using our model of LPS-induced senescence, we found that cholangiocytes expressing the S62A mutant exhibited increased p21 expression (~1.5-fold), increased percentage of cells positive for SA-b-gal (1.5-fold), and reduced proliferation (~50%) compared with experimentally induced senescent DMYC cholangiocytes reconstituted with WT MYC (Figure 10*H and I*). Conversely, cholangiocytes expressing MYC T58A cultured in our model of LPS-induced senescence exhibited decreased p21 expression, (~50% and 75%) and decreased SA-b-gal positivity (~50% and 75%) compared with experimentally induced senescent MYC WT and MYC S62A cholangiocytes, respectively (Figure 10*H and I*). Additionally, we found, using our model of induced senescence, that the MYC T58A cholangiocytes exhibited increased proliferation, as measured by MTS assay, compared with both MYC WT and MYC S62A cholangiocytes (Figure 10*I*). Moreover, treatment of the sen-res clone 28 with the MYC inhibitor, MYCi975, in the presence or absence of senescence inducing stimuli not only induced senescence, but promoted IL6 and IL8 expression, well-known senescence-associated secretory phenotype (SASP) factors, and suppressed the proliferation markers, *KI67* and *PCNA* (Figure 11*A–D*). Together, these results support that post-translational modification of MYC (ie, phosphorylation) is a central mediator driving cholangiocytes towards either a proliferative or senescent cell fate.

GSK3B-mediated MYC T58 Phosphorylation Decreases MYC Expression and Promotes Cholangiocyte Senescence

Canonically, MYC is phosphorylated at T58 by glycogen synthase kinase 3b (GSK3b).[18] We hypothesized that, under LPS-mediated stress, GSK3B promotes MYC T58 phosphorylation and cholangiocyte senescence. Thus, the inhibition of GSK3B should result in MYC stabilization, cholangiocyte resistance to senescence, and increased proliferation. Our RNA-seq data supports that GSK3B mRNA is increased in FACS-isolated senescent cholangiocytes, and immunoblot confirms increased GSK3B protein expression (Figure 12*A and B*). We further show, by immunoblot, that LPS-mediated stress in NHC (mixed population of sen and sen-res) reduced phosphorylation of the inhibitory phosphorylation site on GSK3B Serine 9. However, the addition of the GSK3B inhibitor, CHIR, in the presence of LPS, blocked the reduced Serine 9 phosphorylation. Moreover, CHIR prevented loss of MYC S62 phosphorylation in the presence of LPS and promoted loss of MYC T58 phosphorylation in the presence of LPS. LPS-stressed NHCs exhibited increased senescence (p21 expression) and p16-GFP expression compared with vehicle-treated NHCs, whereas LPS-stressed cholangiocytes cultured in the presence of the GSK3B inhibitor suppressed LPS stress-associated p21 expression and reduced detection of p16-GFP (Figure 12*C and D*). In addition, phosphorylation patterns and senescence detection in the sen-res clone, Clone 28, in the presence of LPS were unaffected by the addition of the GSK3B inhibitor. Conversely, the addition of GSK3B inhibitor in the presence of LPS in the senescent-sensitive clone, Clone 80, blocked the loss of inhibitory phosphorylation (pS9-GSK3B) and reduced the induction of LPS-induced p21 expression and detection of induced p16-GFP expression. Together, these results support that inhibition of GSK3B promotes MYC stabilization (via phospho-MYCS62) and prevents MYC degradation (via phospho-MYCT58). Moreover, these results also support that GSK3B inhibition suppresses the induction of senescence in LPS-induced cholangiocyte senescence.

The GSK3B Inhibitor, CHIR99021, promotes cholangiocyte Proliferation in Mouse Models of PSC

Having demonstrated the functional relevance of GSK3B in cultured NHCs and sen-res and sen-sen cholangiocytes, we next assessed whether pharmacologic inhibition of GSK3B (CHIR99021) would promote cholangiocyte proliferation and increased ductular reaction in the DDC-fed mouse model of biliary injury. We first assessed, by immunofluorescence, portal vs parenchymal cholangiocyte phospho-T58-MYC expression in livers from patients with PSC and DDC-fed and *Mdr2-/-* mice. We found that phospho-T58-MYC expression is increased in portal

Figure 10. (***See previous page***). **Senescent and senescent-resistant cholangiocytes exhibit differential MYC phosphorylation.** (*A*) RNAseq and qPCR show that *MYC* gene expression is elevated in sen-res vs sen cholangiocytes. (*B and C*) Immunoblots of total and phospho-MYC in FACs isolated sen and sen-res cholangiocytes. Total MYC protein is increased in sen-res vs sen cholangiocytes. MYC S62 phosphorylation is increased in FACS isolated sen-res vs sen cholangiocytes, and, conversely, that T58 phosphorylation is increased in the sen vs sen-res population (quantitation in *C*). (*D and E*) Immunoblot of total and phospho-MYC in clonal isolates. Sen-res clone (clone 28), but not the sen-sen clone (clone 80), exhibited increased S62 phosphorylation (~1.5-fold increase), whereas clone 80, but not clone 28, exhibited increased T58 phosphorylation (~2-fold increase) following LPS-mediated stress (quantitation in *E*). (*F*) Immunoblots for MYC, phospho-MYC, and p21 in NHCs and cholangiocytes depleted of MYC (DMYC). D*MYC* cholangiocytes (~70% reduction of MYC), cultured in the absence of LPS insult, exhibited increased p21 expression (~3-fold) compared with WT NHCs cultured in the absence of LPS. (*G*) SA-b-gal-positive cholangiocytes increased ~5-fold, and proliferation, as measured by MTS assay, was reduced by 50% in D*MYC* vs NHC. (*H and I*) MYC, phospho-MYC, and p21 immunoblots in D*MYC* cholangiocytes reconstituted with WT MYC, or phospho mutants S62A MYC, or T58 MYC. MYC S62A exhibited increased LPS-induced p21 expression, an increased percentage of SA-b-gal-positive cells (~5-fold), and diminished proliferation (50%) compared with D*MYC* cholangiocytes reconstituted with WT MYC. Conversely, MYC T58A exhibited decreased LPS-induced p21 expression, (~50% and 75%) and decreased SA-b-gal positivity (~50% and 75%) compared with experimentally induced senescent MYC WT and MYC S62A cholangiocytes.

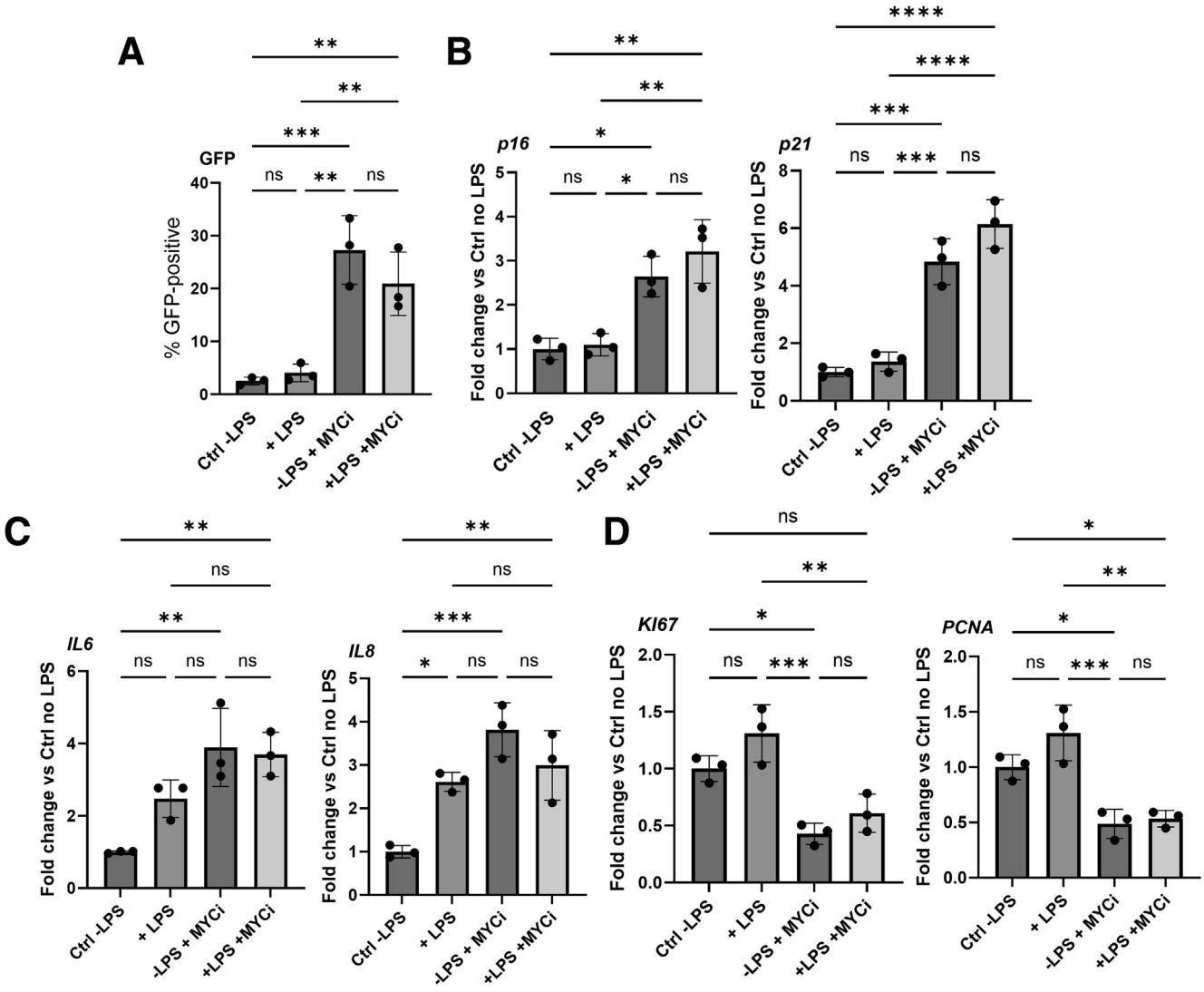

Figure 11. MYC inhibition promotes senescence in the senescecnt resistant clone, clone 28. MYC inhibition (MYCi), in the presence or absence of LPS, promotes: p16 promoter-driven expression of the GFP reporter (*A*); increased mRNA expression of the senescence markers, *p16* and *p21* (*B*); increased expression of the SASP markers, *IL6* and *IL8* (*C*); and decreased expression of the proliferation markers, *KI67* and *PCNA* (*D*).

cholangiocytes in the DDC-fed and *Mdr2-/-* mice (~2-fold) and livers from patients with PSC (~4-fold) compared with cholangiocytes localized to the parenchyma (Figure 13*A*). Picrosirius red staining revealed that DDC-fed and *Mdr2-/-* mice treated with vehicle exhibited increased fibrosis compared with mice fed normal chow. Treatment with the GSK3B inhibitor promoted increased fibrosis in DDC-fed mice (measured by Picrosirius red staining) compared with DDC-fed mice treated with vehicle and trended towards increased fibrosis ($P = .087$) in *Mdr2-/-* mice compared with vehicle-treated *Mdr2-/-* mice (Figure 13*B and C*). We also found that GSK3B inhibitor-treated DDC-fed mice showed increased KRT7-positive cholangiocytes and increased percentage of PCNA-positive cholangiocytes in the ductal and parenchymal areas (ductular reaction) and increased mRNA expression of *Krt7* and *Pcna*, and reduced mRNA expression of the senescence marker *p16* (Figure 13*D and E*). *Mdr2-/-* mice also showed increased KRT7 positivity, PCNA-positive cholangiocytes, and a similar increase of *Krt7* and *Pcna* mRNA and decreased *p16* mRNA expression following GSK3B inhibitor treatment (Figure 13*F and G*). Serum biochemistries revealed elevated total alkaline phosphatase and alanine aminotransferase in the *Mdr2-/-* GSK3B inhibitor-treated mice compared with vehicle-treated mice (Figure 14). Together, these results support that inhibition of GSK3B-mediated phosphorylation of T58-MYC promotes the cholangiocyte proliferative phenotype.

Discussion

The major findings reported here include that post-transcriptional modification of MYC functions as a central driver of the cholangiocyte response to stress and in PSC.

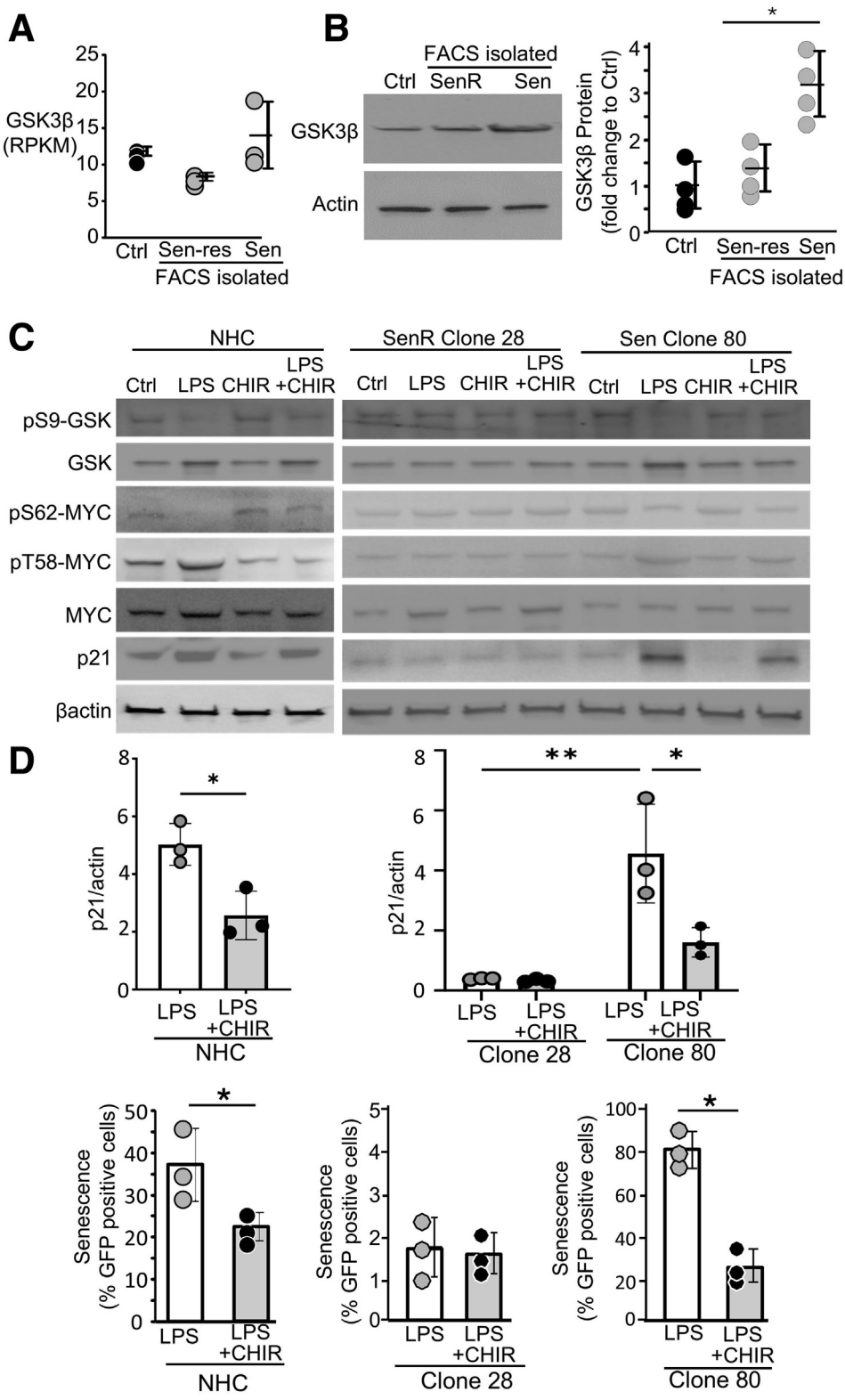

Figure 12. GSK3B decreases MYC expression and promotes cholangiocyte senescence. (*A and B*) RNAseq demonstrates that *GSK3B* mRNA is increased in FACS-isolated senescent cholangiocytes and immunoblot confirms increased GSK3B protein expression. (*C*) Immunoblots showing that LPS-mediated stress in NHC reduced phosphorylation of GSK3B Serine 9 (pS9-CSK3B, inhibitory phospho-site). The GSK3B inhibitor, CHIR, in the presence of LPS, blocked the reduced Serine 9 phosphorylation, prevented loss of MYC S62 phosphorylation, and promoted loss of MYC T58 phosphorylation. Phosphorylation patterns and senescence detection in the sen-res clone, Clone 28, in the presence of LPS were unaffected by the addition of the GSK3B inhibitor. The GSK3B inhibitor in the senescent-sensitive clone, Clone 80, blocked the LPS-induced loss of inhibitory pS9-GSK3B, reduced the induction of LPS-induced p21 expression. (*D*) Quantitation of immunoblot p21 expression and detection of induced p16-GFP expression (marker of senescence). The GSK3B inhibitor suppressed LPS stress-associated p21 expression and reduced detection of p16-GFP in NHC and Clone 80.

Our data support the notion that MYC T58 phosphorylation, by GSK3B, suppresses cholangiocyte proliferation and promotes cholangiocyte senescence. We further demonstrated that MYC inhibitors diminished, while GSK3B inhibitors exacerbated, cholangiocyte proliferation and fibrosis in the DDC-fed and *Mdr2-/-* mouse models. Together, these results

reveal a kinase mediator of cholangiocyte cell fate and identify MYC as a "molecular switch" in determining cholangiocyte responses to cellular stress. These findings inform on cholangiocyte heterogeneity and PSC pathogenesis, support that MYC drives cholangiocyte proliferation, and identify a targetable feature of this disease.

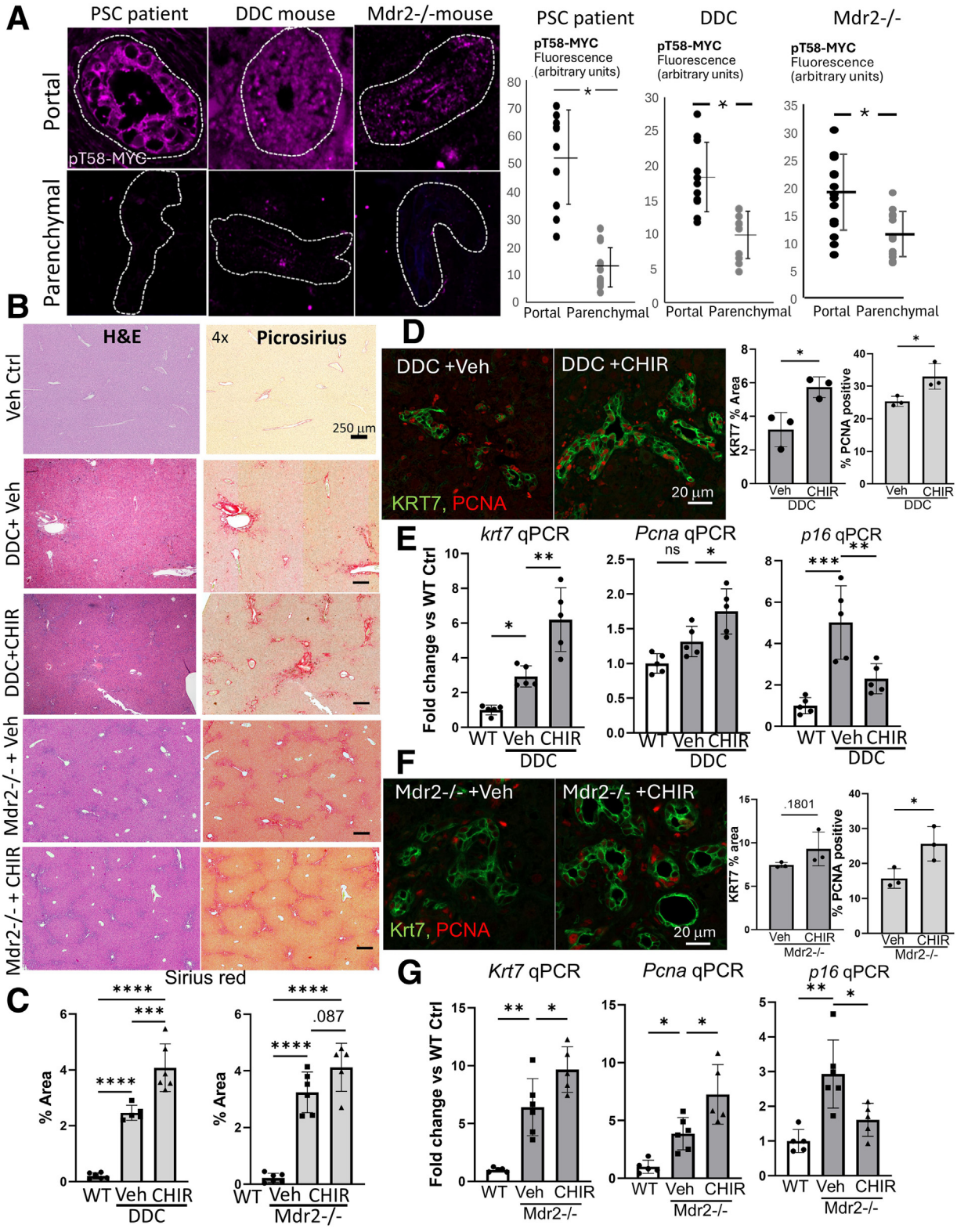

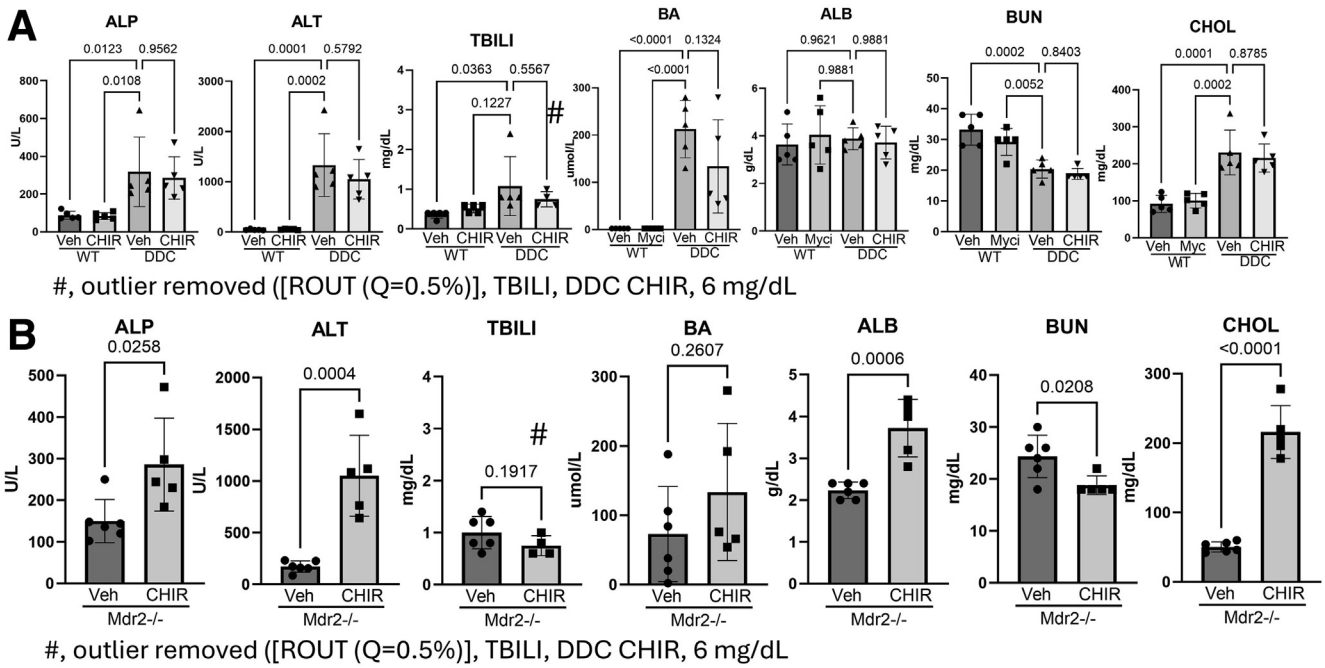

Figure 14. Serum biochemistries in the presence and absence of the GSK3B inhibitor, CHIR99021. (*A*) DDC-fed mice treated with CHIR did not show significant alteration in serum biochemistries compared with DDC-fed vehicle-treated mice. (*B*) *Mdr2-/-* mice treated with CHIR exhibited elevated ALP, ALT, ALB, and CHOL compared with vehicle-treated *Mdr2-/-* mice.

In response to injury, reactive cholangiocytes proliferate and are integral to establishing the ductular reaction (DR), a common feature of cholestatic liver diseases. Histologically, the DR is observed as an expansion of biliary ductules into the liver parenchyma, accompanied by a mixed inflammatory infiltrate and increased matrix deposition.[19] The cholangiocytes within the DR are predominantly derived from proliferation of pre-existing cholangiocytes; alternatively, expansion of liver progenitor cells or transdifferentiated hepatocytes have been shown to contribute to the DR, likely depending on the extent and cause of injury.[20–22] Physiologically, the DR is likely initiated to promote liver regeneration and as a compensatory response to loss of functioning bile ducts.[23] Pathophysiologically, extensive DR correlates with disease state and development of cirrhosis.[21,23,24] Several prominent signaling pathways have been implicated in driving the DR, including Notch receptor 1 (NOTCH1), HIPPO/Yes associated protein (YAP), and WNT/b catenin signaling pathways.[25–29] These pathways have been shown to drive bile duct morphogenesis during development and expansion of liver progenitor cells during liver injury. Here we identify MYC as a prominent driver of the DR in liver injury. The interplay between the above signaling pathways and MYC activation in PSC merits further investigation.

In this study, we demonstrated that LPS, H_2O_2, and IR promoted NHC senescence in ~40% of the cells. In a previous study, we demonstrated that LPS, a gram-negative bacterial cell wall component that drives an innate immune response through toll-like receptor 4 signaling, promotes NHC senescence via activation of N-Ras.[6] Repeated H_2O_2 treatment, which promotes prolonged oxidative stress,

Figure 13. (*See previous page*). The GSK3B Inhibitor, CHIR, promotes cholangiocyte proliferation in mouse models of PSC. (*A*) Immunofluorescence of T58-MYC in portal vs parenchymal cholangiocyte in livers from patients with PSC and DDC-fed and *Mdr2-/-* mice. T58-MYC expression is increased in portal compared with parenchymal cholangiocytes in livers from patients with PSC (~4-fold) and both mouse models (~2-fold). (*B*) Representative images of H&E-stained liver sections showing parenchyma and portal tracts of vehicle-treated WT control (Veh Ctrl; n = 6), DDC-fed plus vehicle (n = 6), and DDC-fed GSK3B inhibitor (CHIR) treated mice (n = 6; *left panels*) and Picrosirius red-stained liver sections showing deposition of collagen (*right panels*). (*C*) Quantitation of Picrosirius red reveals a significant increase in fibrosis in CHIR-treated DDC-fed mice and a trend towards significance ($P = .087$) in CHIR treated *Mdr2-/-* mice. Data is presented as percentage of Picrosirius positive/total image area. (*D*) Immunofluorescence of KRT7 and PCNA in DDC-fed mice. KRT7 (KRT7 positive/total image area) and percentage of cholangiocytes positive for PCNA were increased in mice treated with the GSK3B inhibitor, CHIR. (*E*) qPCR for total liver *Krt7*, *Pcna*, and *p16* in WT C57BL6, DDC-fed, and DDC-fed CHIR-treated mice. Total liver *Krt7* and *Pcna* mRNA are increased, whereas total liver *p16* is decreased in CHIR-treated DDC-fed vs DDC-fed vehicle-treated mice. (*F*) Immunofluorescence of KRT7 and PCNA in *Mdr2-/-* mice. Total KRT7 trended towards a significant increase ($P = .164$), and the percentage of cholangiocytes positive for PCNA was increased in *Mdr2-/-* mice treated with CHIR. (*G*) qPCR for total liver *Krt7*, *Pcna*, and *p16* in WT C57BL6, *Mdr2-/-*, and *Mdr2-/-* CHIR-treated mice. Total liver *Krt7* and *Pcna* mRNA are increased, whereas total liver *p16* is decreased in CHIR treated *Mdr2-/-* vs veh-treated *Mdr2-/-* mice.

and g-irradiation, which directly induces DNA damage, also drive NHC senescence in ∼40% of the NHC as demonstrated by SA-b-Gal staining. Each of the stressors further promoted expression of the cell cycle inhibitors, p21 and p16, and the proinflammatory mediators, IL6 and IL8. Others have shown that different stressors drive distinct features of cellular senescence in hepatocytes, including the SASP.[30] Although not explored in this study, the varied inducers of cholangiocyte senescence likely promote distinct phenotypic features in the senescent cholangiocytes and is an area of interest with pathologic relevance. Moreover, we have previously shown that the endogenous stressor oxysterol cholestane-3β, 5α, 6α-triol (25 mM) also induced significant (∼40%) NHC senescence, whereas the secondary bile acids deoxycholic (25 mM) and lithocholic (10 mM) acid did not.[6] It should be noted, however, that others have demonstrated that glycochenodeoxycholic acid (200 mM) promotes cultured mouse cholangiocyte senescence.[31] The role of bile acids in the induction of cholangiocyte senescence, as well as a disrupted "bicarbonate umbrella" that protects biliary epithelia from the caustic effects of bile acids, also merits further exploration.

Despite the well-characterized role of MYC in numerous cancers and cellular stemness, to date, there is limited information linking MYC to cholangiocyte cellular fate in response to stress and in the ductular reaction. Our data is the first to suggest that MYC post-transcriptional modification (ie, phosphorylation state) functions as a molecular switch driving cholangiocyte proliferation or senescence. MYC is a potent transcription factor that regulates diverse cellular phenotypes including proliferation, senescence, apoptosis, and differentiation.[32,33] The MYC protein is subject to phospho-regulation. Canonically, phosphorylation of MYC S62 (pS62), by mitogen activated protein kinases 1, 2, and 8 (ie, ERK1/2 and JNK), as well as cyclin-dependent protein kinases 2 and 5 (CDK2/5) stabilizes the MYC protein and promotes MYC function as a driver of transcription. Phosphorylated S62 also serves as a priming site for GSK3B phosphorylation of T58 (pT58), which enhances MYC degradation via ubiquitination and proteasomal degradation, thus terminating MYC-driven cellular processes.[34–37] Our data support that, in both senescent NHCs and PSC patient-derived cholangiocytes, MYC-driven gene expression is diminished; conversely, proliferating, senescent-resistant NHCs exhibit increased MYC pathway activation. Moreover, sen and sen-res cholangiocytes exhibit overlapping but distinct secretomes that may inform on cellular communication networks that drive pathologic features of PSC including periductal vs bridging fibrosis. Additionally, in our in vitro model of induced cholangiocyte senescence, we demonstrated that site directed mutagenesis of S62 to alanine (S62A; ie, non-phosphorylatable mutant) diminished cholangiocyte proliferation, whereas mutation of T58 to alanine (T58A) increased proliferation and diminished senescence. These results suggest that loss of pS62 MYC (active) is associated with decreased stress-induced proliferation, whereas loss of pT58 MYC maintains the cholangiocyte in a proliferative state and suppresses senescence.

Of interest, our use of clonally isolated NHCs revealed 2 functionally distinct populations of cholangiocytes; those that are susceptible or resistant to stress-induced senescence. Although the mechanisms driving this phenotypic difference remain to be determined, we propose that individual cholangiocytes are epigenetically primed to proliferate or become senescent. Functionally, both cell fates could play a beneficial role in reparative processes in an injured liver; senescence/SASP prevents expansion of a damaged cell and recruits additional cell types for their removal and reparative processes, whereas proliferative cholangiocytes replace the loss of damaged bile ducts.[8] However, pathophysiologically, persistence of senescent cholangiocytes and continued proliferation of ductular reactive cholangiocytes likely drive periportal and bridging fibrosis, respectively. How the epigenetic profiles of senescent-resistant or -sensitive cholangiocytes establish kinase cascades that either promote proliferation or senescence (via MYC destabilization) require further investigation. The complimentary use of single-cell RNA-seq and epigenetic profiling (eg, assay for transposase-accessible chromatin using sequencing, ATACseq) of cholangiocytes, both from our in vitro model of induced senescence and those derived from patients with PSC will provide novel insights into cholangiocyte heterogeneity and remain a focus of our ongoing efforts.

We further addressed the functional relevance of MYC in the cholangiocyte response to stress in in vivo models of PSC. We demonstrated that MYC inhibition (MYCi975) suppressed cholangiocyte proliferation and diminished the DR. Fibrosis (Sirius red) was clearly reduced in the DDC-fed mouse model, whereas *Mdr2-/-* mice trended towards significantly diminished fibrosis. We propose that this difference between the 2 mouse models may be due to the extent of liver damage at the time of MYCi975 intervention as well as the acute (DDC) vs chronic (*Mdr2-/-*) deposition of collagen. With the demonstration that MYC inhibition diminished cholangiocyte expansion into the parenchyma and associated fibrotic processes, we proposed that persistent MYC activation, via the suppression of T58 phosphorylation by GSK3B inhibition, would have an opposite effect and promote cholangiocyte proliferation, ductular reaction, and bridging fibrosis. Indeed, we found that the inhibition of GSK3B promoted expansion of cholangiocytes into the liver parenchyma and increased bridging fibrosis. These results are in line with previous studies showing the functional relevance of T58 phosphorylation in suppressing proliferation and the transforming capabilities of MYC.[34,36,38]

In conclusion, we have defined a role of MYC protein in the cholangiocyte cellular fate in response to biliary injury. We provide evidence that the phosphorylation state of MYC functions as a "molecular switch" that determines whether a cholangiocyte withdraws from the cell cycle (senesces) or proliferates, 2 opposite, yet potentially pathologic cellular fates. Our data also supports a major role of the kinase, GSK3B, in driving the senescent cell fate. Although the DR may have beneficial effects in early-stage cholangiopathies (ie, replacing bile duct mass), it is increasingly clear that this has detrimental effects in late-stage disease.[23] The DR

remains a complex, ill-defined pathologic process in the cholangiopathies. These data support that regulation of MYC function via upstream kinase drivers of MYC function may have therapeutic benefits. Additionally, these results may be generalizable to other cholangiopathies and liver diseases with profound ductular reaction including primary biliary cirrhosis, biliary atresia, alcoholic- and non-alcoholic associated metabolic dysfunction-associated fatty liver disease.

Methods

Experimental Procedures

This study was approved by the Mayo Clinic Institutional Review Board and abides by the Declaration of Helsinki principles. The Mayo Clinic Institutional Animal Care and Use Committee also approved this study.

Animal Experiments

C57BL/6 WT mice were obtained from Charles River. ATP binding cassette subfamily B member 4 (*Abcb4*) knockout (C57BL/6-*Mdr2-/-*) mice were a gift from Dr Oude Elferink (Tytgat Institute). Mice were housed at the Mayo Clinic animal care facility with a standard 12:12-hour light/dark cycle and ad libitum access to water and standard rodent diet as previously described.[39] We used female C57BL/6 mice for the DDC experiments. Beginning at 7 weeks of age, mice received either a chow diet supplemented with 0.1% DDC (4 days DDC diet, 3 days standard chow) or standard chow for 7 weeks. Beginning at 11 weeks of age, DDC diet-fed (6–8 mice per group) and *Mdr2-/-* mice (6 mice per group) were treated by intraperitoneal injection of the MYC inhibitor (MYCi975: 50 mg/kg) or the GSK3 inhibitor (CHIR99021: 10 mg/kg) 3 times per week for 3 weeks. Mice were sacrificed, and livers were processed for further analysis.

Liver Tissues

Human PSC patient samples, which fulfilled clinical, serologic, histologic, and/or cholangiographic criteria for stage IV PSC, were obtained at the time of transplant. All patients with PSC were negative for biochemical, imaging, or histologic evidence of cholangiocarcinoma. Normal liver samples from surgical resection or explant were also utilized. Liver specimens were fixed in 10% neutral buffered formalin, embedded in paraffin, and sectioned (5 μm) for immunofluorescence.

Cholangiocytes were also isolated from fresh liver explant tissue from patients (2 male and 1 female; ages 46, 57, and 58, respectively) with stage IV PSC without cholangiocarcinoma. The isolation was performed, as described previously, through a series of digestion, filtration, and bead isolations steps.[7] Briefly, explanted tissue ($\sim$1 cm^3) was finely cut using sterile razor blades, incubated in Dulbecco's modified Eagle medium (DMEM) containing fetal bovine serum, penicillin/streptomycin, bovine serum albumin, collagenase, and DNase for 45 minutes in a shaking water bath at 37 °C. The digested tissue was filtered first through a 100-mm filter and subsequently through a 40-mm filter. Cells retained in the 40 mm filter were washed with DMEM and further digested with DMEM containing hyaluronidase for 30 minutes at 37 °C. The cells were plated on collagen-coated flasks overnight. Cholangiocytes were bead isolated using Epithelial Enrich magnetic bead isolation kit (Life Technologies) and replated on collagen-coated flasks. Cholangiocytes were also isolated from 3 C57BL/6 and 3 C57BL/6-*Mdr2-/-* 12-week-old female mice using this same protocol. Briefly, mice were humanely sacrificed at 12 weeks of age, an age in which *Mdr2-/-* mice exhibit biliary fibrosis and ductular reaction,[39] and livers were processed as above.

Cell Sorting

NHCs were stably transfected with a CDKN2A (ie, *p16*) promoter-driven GFP reporter (*p16*-GFP-NHC[39]; further details provided in Supplementary Material) and cultured in the presence or absence of cellular stressors in our in vitro model of experimentally induced NHC senescence (see below). The cells were trypisinized, washed once with 1$\times$ phosphate buffered saline (PBS), resuspended in ice cold 1$\times$ PBS, and standard FACS analysis was performed. The PSC patient primary cholangiocytes and mouse cholangiocytes were sorted using a fluorogenic substrate, C12FDG (5-dodecanoylaminofluorescein di-β-D-galactopyranoside; Invitrogen), to assess SA-βgal activity. Briefly, isolated cholangiocytes were washed once in 1$\times$ Hank's Balanced Salt Solution (HBSS), treated with 100 nM Bafilomycin A1 in NHC media for 1 hour to normalize the lysosomal to pH 6.0. C12FDG was added to a final concentration of 33 μM and incubated for an additional 1 hour. The cells were then centrifuged for 5 minutes at 1000 rpm, washed, and resuspended as above, and FACS analyses were performed.

Cell Culture and In Vitro Model of Senescence

The well-characterized NHC cell line derived from normal liver was provided by Dr Medina (University of Navarra).[40] The NHC cells were routinely monitored for mycoplasma using Lonza MycoAlert and cultured in the presence of Primocin (Invivogen). Our in vitro model of senescence was performed as previously described.[4–6] Briefly, cholangiocytes (NHCs) were induced to senescence with IR (10 Gy)[41] or repeated exposure to LPS (200 ng/mL) or H_2O_2 (50 nM) over 10 days.[6] For the SA–β-gal assay, cells were grown in 12-well plates, washed, fixed, and stained with SA–β-gal using the Cell Signaling Cellular Senescence Detection Kit per manufacturer's direction. Briefly, following senescence induction, the cholangiocytes were washed with PBS, fixed with 25% glutaraldehyde, washed with PBS, and treated overnight with a staining solution containing X-Gal. The percentage of senescent cells was determined by manual counting using a 20$\times$ objective and bright field illumination of 5 randomly selected areas.

Chromatin Immunoprecipitation-PCR

Chromatin immunoprecipitation (ChIP) was performed as previously described.[4] Briefly, pmmunoprecipitations were performed with the total MYC (Abcam, clone E5Q6W)

antibody. qPCR was performed in a Rotor-Gene Q (Qiagen) system using Rotor-Gene SYBR Green master mix (Qiagen) according to manufacturer's directions and using primers described in Supplementary Table 3.

Generation of MYC Phospho Mutants (S61A/T58A MYC)

pcDNA3-cmyc was a gift from Wafik El-Deiry (Addgene plasmid: 16011; http://n2t.net/addgene:16011; RRID: Addgene_16011). The pcDNA3-cmyc contains the MYC open reading frame and was used as a template to generate the T58A and S62A MYC mutants. We used the Q5 site-directed mutagenesis (SDM) kit (New England BioLabs). Briefly, PCR primers were designed using the NEBaseChanger (New England BioLabs) algorithm. Both the T58A and S62A SDM constructs substituted a base pair, which results in the non-phosphorylatable form of MYC. Primers used for SDM are found in Supplementary Table 3. PCR for the site-directed mutants was carried out using the following parameters: 98 °C for 10 seconds, 25 cycles of 98 °C for 10 seconds, 70 °C (T58A and S62A primers) for 60 seconds, 72 °C for 4 minutes, and 72 °C for 30 seconds. DNA sequence confirmation was performed on all plasmid constructs at the GeneWiz Sequencing Facility.

Cell Dilutional Cloning

To achieve individual clonal cells stably transfected with p16-GFP-NHC, cells were trypsinized and counted. The cells were seeded at a density of 0.5 cells/well in a 96-well plate and allowed to grow in complete media. Any wells that appeared to contain multiple cells after the initial seeding or multiple different clones were excluded from the experiment. After the cells had grown to near confluency in the 96-well dish, the cells were passaged, and part of the clone was grown up in complete media and cryostored, whereas the other portion of the same clone was used in the in vitro model of senescence (complete media +LPS [200 ng/mL] for 10 days).

Gene Set Enrichment

Bioinformatics analysis was performed on RNA-seq datasets to assess differentially expressed genes between NHCs and PSC patient-derived cholangiocytes as well as between FACS-isolated senescent and senescent-resistant cholangiocytes. Briefly, total RNA-seq datasets were uploaded into Qiagen's IPA software for core analysis and global molecular network analysis using the Ingenuity pathway knowledge base. IPA identified canonical pathways, upstream activators, and gene networks.

Total RNA Extraction and qRT-PCR

TRIzol (Invitrogen) was used to extract total RNA from the NHC cells according to the manufacturer's protocol. Following RNA extraction, 1.0 μg of total RNA was used as template for reverse transcription (RT) using the SuperScript III First Strand Synthesis system (Invitrogen). The cDNA was then used as template for PCR amplification (primers listed in Supplementary Table 3), mixed with the Rotor-Gene SYBR Green PCR Master Mix (Qiagen), and analyzed with the Rotor-gene quantitative PCR instrument (Qiagen). All qPCR samples were normalized to 18s RNA.

Protein Isolation and Western Blotting

Protein lysate was harvested from NHC cells and subjected to electrophoresis on SDS-PAGE gels. The following primary antibodies used: p21 Waf1/Cip1 (clone 12D1), total MYC (clone E5Q6W), pS62-MYC (clone E1J4K), pT58-MYC (clone E472K), total GSK (clone D5C5Z) and pS9-GSK (clone D3A4) (Cell Signaling) and ActB (Sc-1615; Santa Cruz Biotechnology). The membranes were washed and incubated with secondary antibodies conjugated to HRP (1:2000 dilution, Cell Signaling). Western blotting bands were detected using Enhanced Chemiluminescent plus detection system (ECL Plus; Promega).

Immunofluorescence

Briefly, tissue sections were deparaffinized in xylene and rehydrated through a series of increasing ethanol dilutions. All subsequent steps were performed for standard immunofluorescence assays. Primary antibodies for immunofluorescence staining were p16 (ThermoFisher; clone PA5-20379), PCNA (Santa Cruz Biotechnology; clone PC10), total MYC (Cell Signaling; clone E5Q6W), pT58-MYC (Cell Signaling; clone E472K), and KRT7 (Santa Cruz Biotechnology; clone LP1K) overnight at 4 °C. After primary incubation, slides were washed in PBS and incubated with Alexa Fluor secondary antibodies (Life Technologies) for 60 minutes at room temperature. For quantification of percent area of KRT7+ fluorescence intensity of parenchymal cholangiocytes (ductular reaction), we used ImageJ software; to quantitate percent PCNA positive KRT7+ cholangiocytes in our regions of interest, we used Zen Blue Imaging software and manual counting.

Transfection and Generation of Stable Cell Lines

NHC cells were transfected with CDKN2A (p16) promoter cloned upstream of eGFP in pEZX-PFO2 (p16-GFP), this plasmid was purchased from Genecopoeia (catalog HPRM54678-PF02). This plasmid consists of ~1000 bp putative promoter region of CDKN2A transcript variant 1. The transfected cells were selected using puromycin (1.5 μg/mL) for 7 days. Following puromycin selection, the media was replaced with complete NHC media and continued incubation at 37 °C. For MYC deletion studies, the MYC double nickase plasmid pair was purchased from Santa Cruz Biotechnology, Inc. (sc-400001-NIC). Each of the 2 plasmids contains a D10A mutated Cas9 nuclease and a unique MYC-specific 20-nucleotide guide RNA to allow for highly specific gene knockout. One of the plasmids also contains a GFP tag, whereas the second plasmid contains a puromycin resistance cassette allowing for visualization and selection of the cotransfected cells. NHCs were transfected with the double nickase plasmid using FuGENE HD (Promega). On the day of transfections, the NHCs were 60% to 70% confluent. The transfection mix (2 μg of plasmid + 8 μL of FuGENE HD in 100 μL of Optimem; Invitrogen) was added to the cells. Following 24 hours of incubation, the transfection medium

was removed and replaced with complete medium, and the cells were incubated for 24 hours. Next, the complete medium was replaced with complete medium containing 1.5 μg/mL of puromycin. After a week on selection, only transfected cells remained viable, and the medium was switched to complete medium in the absence of puromycin. Following MYC double nickase stable transfection, the cells were co-transfected with the following plasmids: WT-MYC (consisting of a functional open reading frame), MYC T58A-phosphomutant, or MYC S62A-phosphomutant. After using the above protocol for transfection, co-transfected cells were selected using G418 (1500 μg/ml) for 2 weeks. For FACS, the transfected cells were sorted using a BDFACS Aria. Cell yield, composition, and FACS plots were further assessed using the FlowJo software.

Reactive Oxygen Species Assay

FACS-sorted senescent-resistant (no GFP), and senescent-sensitive (+GFP) cells were plated at a density of 5.0×10^5 cells per well of a 96-well plate for 24 hours at 37 ^{o}C. The total reactive oxygen species (ROS) of the cells were determined using Abcam's Cellular ROS Detection Kit (Red fluorescence) (ab186027) according to the manufacturer's directions.

Mitochondrial Staining

Mitochondrial staining was achieved using Mitotracker Red FM (ThermoFisher) and Mitoview 633 (Biotium). Mitotracker Red FM was used to analyze the difference between sen and sen-res mitochondrial mass, whereas Mitoview 633 was used to determine differences in mitochondrial membrane potential. Experiments were performed according to manufacturers' directions.

Statistical Analysis

Data are presented as mean ± standard deviation (SD), unless otherwise noted. Student's *t*-test (2-tailed), and 1-way analysis of variance (ANOVA) with Tukey's test evaluated statistical significance with GraphPad Prism 9.1 software (GraphPad Software, Inc). All in vitro studies were carried out independently a minimum of 3 times. Animal studies used no fewer than n = 6 per group. Within the figures, asterisks denote $*P < .05$; $**P < .01$; $***P < .001$; $****P < .0001$; and n.s, not significant. All authors had access to the study data and approved of the final manuscript.

Supplementary Material

Note: To access the supplementary material accompanying this article, visit the full text version at https://doi.org/10.1016/j.jcmgh.2025.101547.

References

1. Karlsen TH, Folseraas T, Thorburn D, Vesterhus M. Primary sclerosing cholangitis - a comprehensive review. J Hepatol 2017;67:1298–1323.
2. Lazaridis KN, LaRusso NF. Primary sclerosing cholangitis. N Engl J Med 2016;375:2501–2502.
3. Bambha K, Kim WR, Talwalkar J, et al. Incidence, clinical spectrum, and outcomes of primary sclerosing cholangitis in a United States community. Gastroenterology 2003;125:1364–1369.
4. O'Hara SP, Splinter PL, Trussoni CE, et al. The transcription factor ETS1 promotes apoptosis resistance of senescent cholangiocytes by epigenetically up-regulating the apoptosis suppressor BCL2L1. J Biol Chem 2019;294:18698–18713.
5. O'Hara SP, Splinter PL, Trussoni CE, et al. ETS Proto-oncogene 1 transcriptionally up-regulates the cholangiocyte senescence-associated protein cyclin-dependent kinase inhibitor 2A. J Biol Chem 2017;292:4833–4846.
6. Tabibian JH, O'Hara SP, Splinter PL, et al. Cholangiocyte senescence by way of N-ras activation is a characteristic of primary sclerosing cholangitis. Hepatology 2014;59:2263–2275.
7. Tabibian JH, Trussoni CE, O'Hara SP, et al. Characterization of cultured cholangiocytes isolated from livers of patients with primary sclerosing cholangitis. Lab Invest 2014;94:1126–1133.
8. Guicciardi ME, Trussoni CE, LaRusso NF, Gores GJ. The spectrum of reactive cholangiocytes in primary sclerosing cholangitis. Hepatology 2020;71:741–748.
9. Alpini G, Glaser S, Robertson W, et al. Large but not small intrahepatic bile ducts are involved in secretin-regulated ductal bile secretion. Am J Physiol 1997;272:G1064–G1074.
10. Benedetti A, Bassotti C, Rapino K, et al. A morphometric study of the epithelium lining the rat intrahepatic biliary tree. J Hepatol 1996;24:335–342.
11. Glaser SS, Gaudio E, Rao A, et al. Morphological and functional heterogeneity of the mouse intrahepatic biliary epithelium. Lab Invest 2009;89:456–469.
12. Andrews TS, Atif J, Liu JC, et al. Single-cell, single-nucleus, and spatial RNA sequencing of the human liver identifies cholangiocyte and mesenchymal heterogeneity. Hepatol Commun 2022;6:821–840.
13. Mootha VK, Lindgren CM, Eriksson KF, et al. PGC-1alpha-responsive genes involved in oxidative phosphorylation are coordinately downregulated in human diabetes. Nat Genet 2003;34:267–273.
14. Subramanian A, Tamayo P, Mootha VK, et al. Gene set enrichment analysis: a knowledge-based approach for interpreting genome-wide expression profiles. Proc Natl Acad Sci U S A 2005;102:15545–15550.
15. Liberzon A, Birger C, Thorvaldsdottir H, et al. The Molecular Signatures Database (MSigDB) hallmark gene set collection. Cell Syst 2015;1:417–425.
16. Sears RC. The life cycle of C-myc: from synthesis to degradation. Cell Cycle 2004;3:1133–1137.
17. Welcker M, Orian A, Jin J, et al. The Fbw7 tumor suppressor regulates glycogen synthase kinase 3 phosphorylation-dependent c-Myc protein degradation. Proc Natl Acad Sci U S A 2004;101:9085–9090.
18. Gregory MA, Qi Y, Hann SR. Phosphorylation by glycogen synthase kinase-3 controls c-myc proteolysis and subnuclear localization. J Biol Chem 2003;278:51606–51612.

19. Roskams TA, Theise ND, Balabaud C, et al. Nomenclature of the finer branches of the biliary tree: canals, ductules, and ductular reactions in human livers. Hepatology 2004;39:1739–1745.
20. LeSage GD, Benedetti A, Glaser S, et al. Acute carbon tetrachloride feeding selectively damages large, but not small, cholangiocytes from normal rat liver. Hepatology 1999;29:307–319.
21. Mavila N, Siraganahalli Eshwaraiah M, Kennedy J. Ductular reactions in liver injury, regeneration, and disease progression-an overview. Cells 2024;13:579.
22. Michalopoulos GK, Barua L, Bowen WC. Transdifferentiation of rat hepatocytes into biliary cells after bile duct ligation and toxic biliary injury. Hepatology 2005;41:535–544.
23. Banales JM, Huebert RC, Karlsen T, et al. Cholangiocyte pathobiology. Nat Rev Gastroenterol Hepatol 2019;16:269–281.
24. Yoshizawa T, Lee JW, Hong SM, et al. Three-dimensional analysis of ductular reactions and their correlation with liver regeneration and fibrosis. Virchows Arch 2024;484:753–763.
25. Apte U, Thompson MD, Cui S, et al. Wnt/beta-catenin signaling mediates oval cell response in rodents. Hepatology 2008;47:288–295.
26. Bai H, Zhang N, Xu Y, et al. Yes-associated protein regulates the hepatic response after bile duct ligation. Hepatology 2012;56:1097–1107.
27. Lu J, Zhou Y, Hu T, et al. Notch signaling coordinates progenitor cell-mediated biliary regeneration following partial hepatectomy. Sci Rep 2016;6:22754.
28. Okabe H, Yang J, Sylakowski K, et al. Wnt signaling regulates hepatobiliary repair following cholestatic liver injury in mice. Hepatology 2016;64:1652–1666.
29. Zhang X, Du G, Xu Y, et al. Inhibition of notch signaling pathway prevents cholestatic liver fibrosis by decreasing the differentiation of hepatic progenitor cells into cholangiocytes. Lab Invest 2016;96:350–360.
30. Kumar P, Hassan M, Tacke F, Engelmann C. Delineating the heterogeneity of senescence-induced-functional alterations in hepatocytes. Cell Mol Life Sci 2024;81:200.
31. Sasaki M, Sato Y, Nakanuma Y. Interferon-induced protein with tetratricopeptide repeats 3 may be a key factor in primary biliary cholangitis. Sci Rep 2021;11:11413.
32. Afifi MM, Crncec A, Cornwell JA, et al. Irreversible cell cycle exit associated with senescence is mediated by constitutive MYC degradation. Cell Rep 2023;42:113079.
33. Meyer N, Penn LZ. Reflecting on 25 years with MYC. Nat Rev Cancer 2008;8:976–990.
34. Henriksson M, Bakardjiev A, Klein G, Luscher B. Phosphorylation sites mapping in the N-terminal domain of c-myc modulate its transforming potential. Oncogene 1993;8:3199–3209.
35. Lutterbach B, Hann SR. Hierarchical phosphorylation at N-terminal transformation-sensitive sites in c-Myc protein is regulated by mitogens and in mitosis. Mol Cell Biol 1994;14:5510–5522.
36. Pulverer BJ, Fisher C, Vousden K, et al. Site-specific modulation of c-Myc cotransformation by residues phosphorylated in vivo. Oncogene 1994;9:59–70.
37. Sears R, Leone G, DeGregori J, Nevins JR. Ras enhances Myc protein stability. Mol Cell 1999;3:169–179.
38. Chang DW, Claassen GF, Hann SR, Cole MD. The c-Myc transactivation domain is a direct modulator of apoptotic versus proliferative signals. Mol Cell Biol 2000;20:4309–4319.
39. Kang JH, Splinter PL, Trussoni CE, et al. The epigenetic reader, bromodomain containing 2, mediates cholangiocyte senescence via interaction with ETS proto-oncogene 1. Gastroenterology 2023;165:228–243.e2.
40. Joplin R, Strain AJ, Neuberger JM. Immuno-isolation and culture of biliary epithelial cells from normal human liver. In Vitro Cell Dev Biol 1989;25:1189–1192.
41. Moncsek A, Al-Suraih MS, Trussoni CE, et al. Targeting senescent cholangiocytes and activated fibroblasts with B-cell lymphoma-extra large inhibitors ameliorates fibrosis in multidrug resistance 2 gene knockout (Mdr2(-/-)) mice. Hepatology 2018;67:247–259.

Received October 21, 2024. Accepted May 23, 2025.

Correspondence
Address correspondence to: Nicholas F. LaRusso, MD, Mayo Clinic, 200 First St SW, Rochester, Minnesota 55905. e-mail: larusso.nicholas@mayo.edu; tel: (507) 284-1006.

Acknowledgments
The authors acknowledge the Mayo Clinic imaging and clinical core, supported by the Center for Cell Signaling in Gastroenterology (P30 DK084567), for providing human tissues and imaging technologies used in this study. This study was further supported by grants from the National Institutes of Health: R01 DK057993 (NFL) and R01 DK0124182 (GJG). This study was also funded by the Chris M. Carlos and Catharine Nicole Jockisch Carlos Endowment in PSC.

CRediT Authorship Contributions
Steven P. O'Hara, PhD (Conceptualization: Equal; Formal analysis: Lead; Funding acquisition: Equal; Investigation: Supporting; Writing – original draft: Lead; Writing – review & editing: Equal)
Patrick L. Splinter, MS (Conceptualization: Supporting; Formal analysis: Supporting; Methodology: Equal; Writing – review & editing: Supporting)
Antonia Felzen, BS (Formal analysis: Supporting; Investigation: Supporting; Writing – review & editing: Supporting)
Carys A. Turner, BS (Investigation: Supporting; Writing – review & editing: Supporting)
Olivia T. Morgenthaler, BS (Investigation: Supporting; Writing – review & editing: Supporting)
Gregory J. Gores, MD (Conceptualization: Supporting; Funding acquisition: Supporting; Supervision: Supporting; Writing – review & editing: Supporting)
Nicholas F. LaRusso, MD (Conceptualization: Equal; Formal analysis: Supporting; Funding acquisition: Equal; Supervision: Lead; Writing – review & editing: Lead)

Conflicts of interest
The authors disclose no conflicts.

Funding
This study was funded by P30 DK084567 (Nicholas F. LaRusso); R01 DK057993 (Nicholas F. LaRusso/Steven P.O'Hara); R01 DK0124182 (Gregory J. Gores); and the Chris M. Carlos and Catharine Nicole Jockisch Carlos Endowment in PSC.

Data Availability
RNA sequencing, Gene Expression Omnibus (GEO) database accession: GSE296039